OPO OPHTHALMIC & PHYSIOLOGICAL OPTICS
THE JOURNAL OF THE COLLEGE OF OPTOMETRISTS

Ophthalmic and Physiological Optics ISSN 0275-5408

FEATURE ISSUE ARTICLE

# Cones in ageing and harsh environments: the neural economy hypothesis

Ann E Elsner, Joel A Papay, Kirby D Johnston, Lucie Sawides, Alberto de Castro, Brett J King, Durand W Jones, Christopher A Clark, Thomas J Gast and Stephen A Burns

Indiana University, Bloomington, USA

**Citation information:** Elsner AE, Papay JA, Johnston KD, Sawides L, de Castro A, King BJ, Jones DW, Clark CA, Gast TJ & Burns SA. Cones in ageing and harsh environments: the neural economy hypothesis. *Ophthalmic Physiol Opt* 2020; 40: 88–116. https://doi.org/10.1111/opo.12670

**Keywords:** ageing, age-related macular degeneration, cones, photoreceptor/retinal pigment epithelial cell complex, retinal degeneration

*Correspondence: Ann E Elsner
E-mail address: aeelsner@indiana.edu

Received: 30 August 2019; Accepted: 31 December 2019

**Author contributions:** AEE & SAB: involved in all aspects of study conception and design; data acquisition, analysis and interpretation; and drafting and critically revising the manuscript. JAP: involved in study design and data acquisition, analysis and interpretation. KDJ: involved in data acquisition, analysis and interpretation and critically revising the manuscript. LS, DWJ & CAC: involved in data acquisition and analysis. AdC: involved in data acquisition and analysis and critically revising the manuscript. BJK: involved in study conception, data interpretation and critically revising the manuscript. TJG: involved in data acquisition, analysis and interpretation and critically revising the manuscript.

## Abstract

*Purpose:* Cones are at great risk in a wide variety of retinal diseases, especially when there is a harsh microenvironment and retinal pigment epithelium is damaged. We provide established and new methods for assessing cones and retinal pigment epithelium, together with new results. We investigated conditions under which cones can be imaged and could guide light, despite the proximity of less than ideal retinal pigment epithelium.

*Recent findings:* We used a variety of imaging methods to detect and localise damage to the retinal pigment epithelium. As age-related macular degeneration is a particularly widespread disease, we imaged clinical hallmarks: drusen and hyperpigmentation. Using near infrared light provided improved imaging of the deeper fundus layers. We compared confocal and multiply scattered light images, using both the variation of detection apertures and polarisation analysis. We used optical coherence tomography to examine distances between structures and thickness of retinal layers, as well as identifying damage to the retinal pigment epithelium. We counted cones using adaptive optics scanning laser ophthalmoscopy. We compared the results of five subjects with geographic atrophy to data from a previous normative ageing study.

Using near infrared imaging and layer analysis of optical coherence tomography, the widespread aspect of drusen became evident. Both multiply scattered light imaging and analysis of the volume in the retinal pigment epithelial layer from the optical coherence tomography were effective in localising drusen and hyperpigmentation beneath the photoreceptors. Cone photoreceptors in normal older eyes were shorter than in younger eyes. Cone photoreceptors survived in regions of atrophy, but with greatly reduced and highly variable density. Regular arrays of cones were found in some locations, despite abnormal retinal pigment epithelium. For some subjects, the cone density was significantly greater than normative values in some retinal locations outside the atrophy.

*Summary:* The survival of cones within atrophy is remarkable. The unusually dense packing of cones at some retinal locations outside the atrophy indicates more fluidity in cone distribution than typically thought. Together these findings suggest strategies for therapy that includes preserving cones.

## Introduction

Cones are the photoreceptors chiefly responsible for vision in daylight, providing the first step for fine spatial and spectral detail. Cones are typically thought to depend greatly upon the retinal pigment epithelium (RPE) for metabolic support, phagocytosis, and photopigment regeneration.[1] Cones and cone pathways are at risk for severe damage in slowly progressing conditions such as age-related macular degeneration (AMD)

and high myopia, which damage the RPE and other aspects of cone microenvironment.

A layer of living cones can bridge regions of geographic atrophy (GA), as seen in cross section from B-scans on optical coherence tomography (OCT).[2] The potential for photoreceptors to survive in harsh environments has also been demonstrated by histological results. In an eye with AMD, photoreceptor cell bodies have been documented as surviving in a 'whorl' at the location of severely degenerated RPE, positioned close to large choroidal vessels and thus benefitting from the high concentration of oxygen that has a short distance to diffuse across the thinned deeper fundus layers.[3] In myopic eyes, while there is an absence of Bruch's membrane that indicates an absence of RPE and choriocapillaris and an additional loss of the middle layer of the choroidal vessels, some photoreceptors and a few large choroidal vessels remain in patchy areas.[4] Similarly, histology shows surviving photoreceptors in glaucoma with peripapillary atrophy, at border of the optic nerve head, without RPE but over a large choroidal vessel.[5] These histological findings point to the potential for cones and cone pathways to provide decades of useful vision in patients with AMD or degenerative myopia.

When there is a lack of functioning RPE, photoreceptors that survive must be subserved by other support mechanisms such as Müller cells and other glia, and also must receive oxygen from large choroidal vessels or even retinal vessels. While the role of Müller and other glial cells in the retina has long been known to provide buffering of ions and nutritive functions, there has been little appreciation that cones can survive without a healthy monolayer of RPE cells. Müller cells are involved in the repair and removal of photoreceptor debris, including phagocytocis of cone outer segments of cones, as shown in a variety of studies in humans and animal models.[6] Müller cells can support photopigment recycling, providing conversion of all-trans-retinol to 11-cis-retinal.[7,8] Macrophages also support phagocytocis of photoreceptors, perhaps to a lesser degree.[9] Microglia phagocytose the photoreceptors that signal to them in retinal degeneration models, a process separate from photoreceptor death via apoptosis.[10] Thus, the support cells that are constitutively within the retina, i.e. Müller cells and microglia, or have entered the retina, i.e. macrophages, may repair or remove photoreceptors, reducing the metabolic demands on the retina to maintain dysfunctional neurons.

The findings that some retinal regions are more spared, taken together with the findings of cones that live without normal retinal pigment epithelium, indicate that neurons alter their structure to allow a more economic existence. This paper presents a review of findings and new data to support the Neural Economy Hypothesis: in harsh conditions, cones alter their structure and function but can survive. Cones shorten in both AMD[11] and particularly the outer segments in retinal degenerations,[12] and metabolic disease.[13] Cones have less effective optical density of photopigment following retinal detachment, i.e. the cones are either shortened, distorted, or can produce less photopigment, but this damage is reversed with time following successful re-attachment surgery.[14] In fact, short cones with fewer outer segments due to fewer segments being made or maintained, are known to support vision in humans, because the fovea at birth does not have the long and tightly packed cones of a young adult.[15] In development, the cone inner and outer segments lengthen, and cones migrate towards the central fovea for roughly the first 6 years of life. The Neural Economy Hypothesis offers a translational goal for vision: mitigating the effects of the adverse cone microenvironment that arises from damage to the RPE and degradation of the retinal vascular network, thereby retaining the potential for useful vision.

## Retinal imaging advances to probe cones and their microenvironment

To better characterise the status of photoreceptors and the retinal environment, including pathological changes, advanced imaging techniques were developed. First, appropriate selection of wavelength is one way to optimise image contrast (*Figure* 1). Photographic methods successfully produced high contrast of features with wavelengths less than about 550 nm, particularly for retinal blood vessels, but contrast decreased as wavelength increased, and was extremely poor for near infrared (NIR) light.[16] To improve the imaging of RPE, NIR infrared light is useful because it can penetrate the retina better than visible wavelength light through blood and macular pigment (*Figures* 1–2).[17] Problems with older technology included stray light that reduced contrast in the image, defocus and other aberrations, and a lack of detector sensitivity. The advances in imaging technology discussed below allowed the use of new and robust, solid state NIR light sources such as a Ti:Sapphire[17] and Chr:Li:SaF,[18] as well as a variety of other laser sources and custom light sources. Illumination sources were introduced via separate optical channels according to wavelength range into a custom retinal imaging device, the research Scanning Laser Ophthalmoscope.[19] Light sources not having symmetric and concentrated beam shapes were spatially filtered. The result was that transverse and lateral chromatic aberrations were reduced to achieve a crisp focus on retinal layers for all wavelengths, so that striking differences for retinal structures that can occur at different wavelengths were detected and quantified.[17,19–21]

Second, advances in the detection pathway improved the contrast in retinal images. Optimisation of the device and retinal parameters became possible by using a detector that

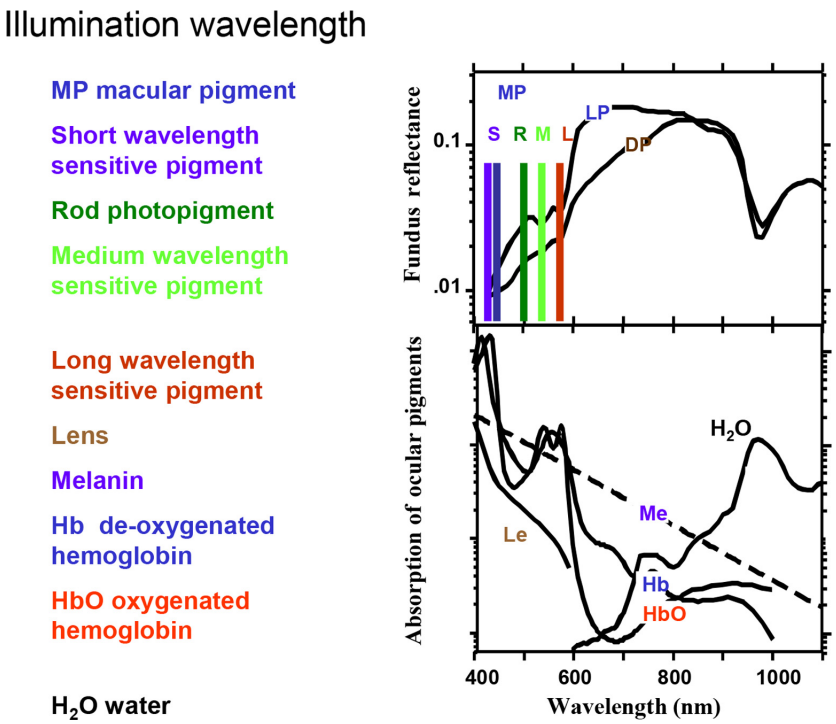


**Figure 1.** The chief absorbers in the normal ocular fundus. Top panel- The peak wavelength of macular pigment absorption, which is similar to that of melanopsin, and the rod and cone photopigments, plotted on a curves of normalised fundus reflection for a lightly pigmented (LP) and darkly pigmented (DP) eye. Adapted from Elsner *et al.*[17]

is robust and sensitive for visible and NIR wavelengths, such as an Avalanche Photodiode, along with increasing stability over time by temperature cooling and a new amplification system with two time constants.[19] The sensitive and stable detection system is crucial for quantitative reflectometry, measurement of changes over time, and analysis of weak signals, so that photopigments and fundus autofluorescence are measureable.[16,19–25]

Modern OCT typically uses NIR illumination to penetrate to the deeper fundus layers, and enhances the weak signals from the eye by interfering the weak signal from the fundus with a stronger reference signal (*Figures* 4–7).[26] While the previous design of OCT devices typically included 830 nm illumination and a Michelson interferometer for signal detection, current methods employ a much wider range of wavelengths, types of lasers, coherence bandwidths, optical designs, and detection methods, allowing deeper penetration, producing improved signal to noise ratio, better axial resolution, and temporal computations.[27–31] The axial resolution of OCT is sufficient to determine borders between retinal layers, which are visualised where there is a focal and sufficiently strong index of refraction change, providing a cross sectional image (B-scan) that shows key anatomical strata and pathological changes (*Figures* 4*a,c,* 5*d,* 6*e,* 7*b*).[32]

Contrast in images is improved compared with fundus photography by using imaging devices that incorporate (1) scanning of the illumination and confocal detection apertures to limit unwanted light from other sources[16] and/or (2) illumination and detection with coherent light using methods such as OCT to boost the signal and allow excellent axial resolution. In scanning techniques, a well-focused and concentrated light source, such as a laser, is swept across the retina and the detection is synchronised with the illumination, and simultaneously constrained to either one point at a time, for example as in a scanning laser ophthalmoscope[19,27,33] or one line at a time, such as in the line-scanning laser ophthalmoscope,[34] the laser scanning digital camera,[35] or the digital light ophthalmoscope (DLO).[36,37] The latter two are wholly digital, in that a two-dimensional detector array is used with one dimensional (line) illumination. Scanning boosts contrast because it eliminates optical cross talk, i.e. the light from more than one area of the retina being sampled at the same location on detector during the sampling, thus confounding the light from different areas on the retina. It does no good to scan light across the retina and then to use a sample-and-hold detector without a method to unmix the light from different retinal areas. The line scan technique can be used on a two dimensional detector, as long as there is a method for separating in

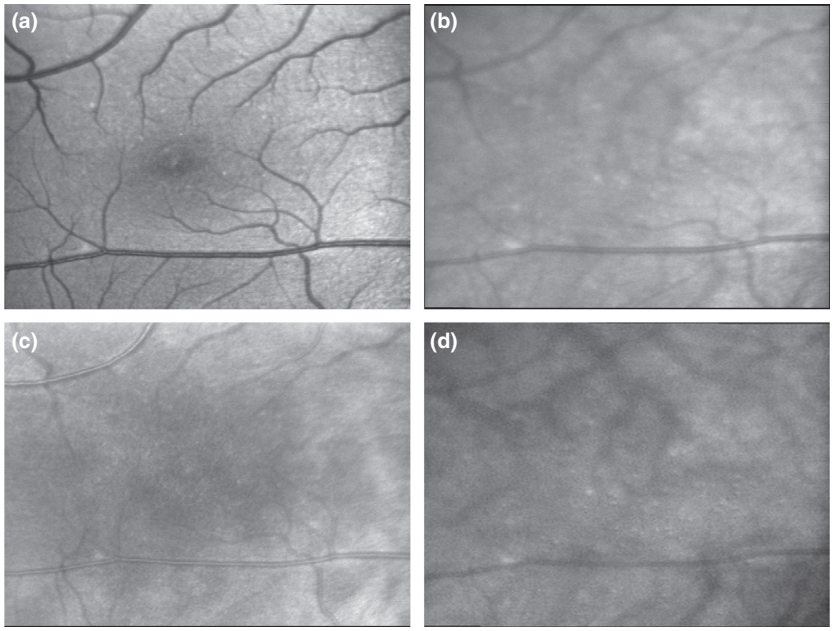


**Figure 2.** Macula of a 40 year old male showing the appearance of early drusen for different wavelengths and imaging modes, using a scanning laser ophthalmoscope. (a) Confocal image at 514 nm, emphasising retinal blood vessels and revealing only a few drusen that are the whitish spots. (b) Confocal image with large aperture at 830 nm, de-emphasising the superficial retinal blood vessels, and emphasising the choroidal blood vessels and many small drusen scattered widely. (c) Confocal image with large aperture at 633 nm, demonstrating visibility of retinal vessels worse than at 514 nm but better than the 830 nm. (d) Multiply scattered light image at 830 nm, showing more drusen than the other imaging conditions, and in which drusen appear as discrete mounds of debris scattered across the macula.

space and/or time the light returning from two or more parts of the retina.[35–37]

## Confocal and multiply scattered light imaging

Contrast and image crispness are improved by the use of confocal apertures, often shaped like pinholes of varying diameters, in a plane conjugate to the retina. The confocal aperture blocks the detection of light from any structure that is not in focus, with light returning directly through the aperture typically providing a stronger signal than the small fraction of light that has bounced off structures many times and by chance passes through the aperture.[16,17] The light that returns directly is also referred to as a specular reflection, backscatter, or singly scattered. There is a large index of refraction difference between lipid and neighbouring retinal tissue, such as produced by drusen, so that the light return from drusen results in a bright spot in a confocal retinal image (*Figures* 2*a,b,* 3*a,* 5*a,* 6*a,* 7*a*).

Healthy retinal tissue is well-ordered, supporting transparency, while diseased tissues tend to be disorganised. Thus, useful images may be produced by using multiply scattered light, i.e. the light that scatters off a structure and scatters many times within the fundus, as long as the illumination is limited to a small region. More than one illumination point[17,38,39] or line (*Figure* 5*b*) can be used, providing multiply scattered light images without necessarily varying the detection aperture. For example, the sides of a druse, which is a mound of debris, direct the light elsewhere in the fundus, where it can scatter multiple times. Due to the strong index of refraction difference between the druse and adjacent retina, considerable light may be scattered rather than absorbed.

The visibility of deeper structures can be enhanced by optimising the illumination wavelength or the imaging mode. Drusen, which are a main clinical hallmark and risk factor for AMD, are known to be mounds of debris and inflammatory products built up within Bruch's membrane and also present in the RPE.[40] OCT provides the axial resolution to measure that photoreceptors are shortened over drusen in patients with AMD.[11] Thus, it is important to identify, localise, and quantify drusen. Drusen beneath the shiny retinal surface are revealed better than with more traditional clinical methods when imaged with NIR illumination along in a device that can optimise the detection of multiply scattered light, such as a confocal aperture that blocks the directly backscattered light, (*Figures* 2*d,* 3*b,* 6*b, c*).[17,41,42] With multiply scattered light imaging, drusen first appear as bumps, small and widely spread in any eye of subjects older than 20 years of age, then larger in more

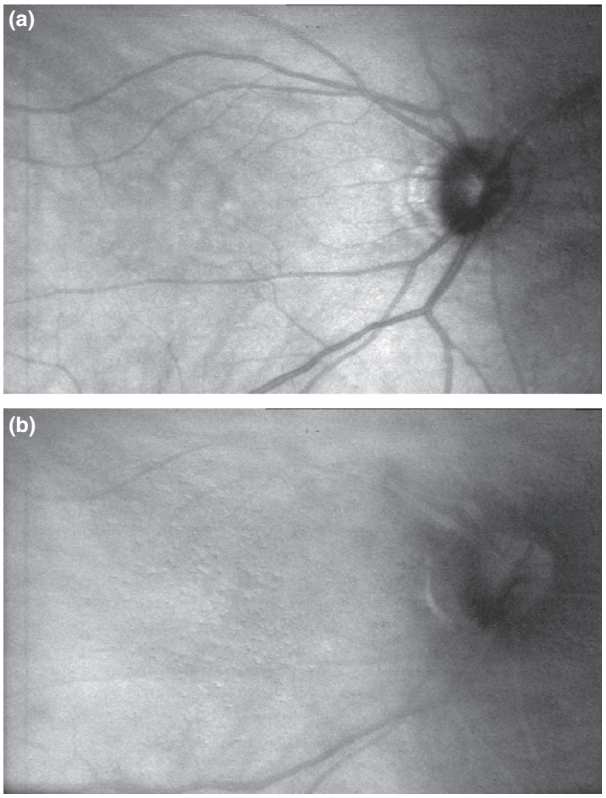


**Figure 3.** Wider field image of the same 40 year old male and same scanning laser ophthalmoscope, showing the appearance of early drusen that are widely scattered and not constrained to just the fovea or a bull's eye pattern. (a) Confocal image at 830 nm. (b) Multiply scattered light image at 830 nm, showing more drusen and with a more three-dimensional appearance than in the confocal image. The multiply scattered light image shows fewer of the retinal blood vessels.

advanced stages of AMD (*Figures* 2 and 3), as documented by fluorescein angiography or colour fundus photography even though these latter methods undersample the pathological changes.[17,42,43] Larger lesions, such as neovascular membranes demonstrated by fluorescein angiography or indocyanine green angiography, can also be better visualised in NIR imaging than in colour fundus photography, with different optical signatures provided by confocal and multiply scattered light.[38,39,41]

RPE hyperpigmentation (*Figure* 5*b*) is the build-up of melanin-containing RPE debris, and when detected on OCT is identified by small, high reflectivity bodies known as hyperreflective foci (*Figure* 5*d*).[44,45] Our multi-modal imaging[45] shows that melanin in hyperpigmentation has both a high index of refraction and the potential for mirror-like reflectivity, along with the expected absorption. While hyperpigmentation is known as an important risk factor for progression to either atrophy or choroidal neovascularisation in AMD, hyperpigmentation is non-specific and also seen in a variety of retinal degenerations that damage the RPE.[44] Photoreceptors lying over RPE that is dead or dying, as documented by hyperpigmentation, are in an extremely harsh microenvironment. Hyperpigmentation is readily seen in eyes with intermediate and advanced AMD.[17,46] However, using wavelengths that match the strong absorption of blood or macular pigment reduces the visibility of drusen and hyperpigmentation, as does using a technique that emphasises the directly returned light from superficial fundus layers (*Figure* 2*a* vs 2*d*).[17,20,21,42] Poor penetration of the illumination may be the reason that drusen were previously underdetected in the fovea or with haemorrhagic lesions. In fact, images in NIR light correspond with the understanding from histology, showing that drusen and other subretinal lesions are widespread,[3] and the most and largest drusen often occur at or near the fovea. The extent and location of drusen puts the cones at risk for decades, not just immediately prior to advanced AMD.

The excellent resolution of OCT allows two particular types of data analysis that define the cone microenvironment. When the retinal layers are segmented, the distances between two or more structures can be computed. OCT axial distance measurements quantify the thickness of the layer containing photoreceptor cell bodies and Müller processes, the outer nuclear layer (ONL). While the extreme loss of photoreceptors is likely to significantly decrease the ONL thickness, older control subjects with fewer cones on average have thicker, not thinner, ONL measurements, which is consistent with retinal remodelling after loss of photoreceptors.[47] This finding also indicates that OCT is not an accurate means of assessing photoreceptor health unless extreme cell loss is expected. Other methods capable of measuring the subtle changes with ageing or disease treatment are needed. However, for understanding structural alterations of the retina on a fine scale in the axial dimension, OCT has a variety of applications. For instance, when there is photoreceptor degeneration, the photoreceptors roll up with support cells, forming structures known as outer retinal tubulation (ORT) (*Figure* 7*b*).[48] ORTs are common in many diseases leading to atrophy, occurring in at least 62% of patients with atrophy in an optometric clinic, and not limited to a tertiary referral center.[49] An ORT can span across regions of atrophy to contact more normal retina and may provide longevity for the cells within it.[49] Not only is ORT readily recognised in OCT B-scans, but the distortions of the outer and inner retina are quantified by measurements of ORT and surrounding retinal structures, using B-scans.[49] The ORT can be more than 1 deg wide, and the inner retina significantly thinned while the outer retina is significantly thickened.

Entire regions of retina can be mapped for a given range of depths and then an OCT slab analysis can elucidate the

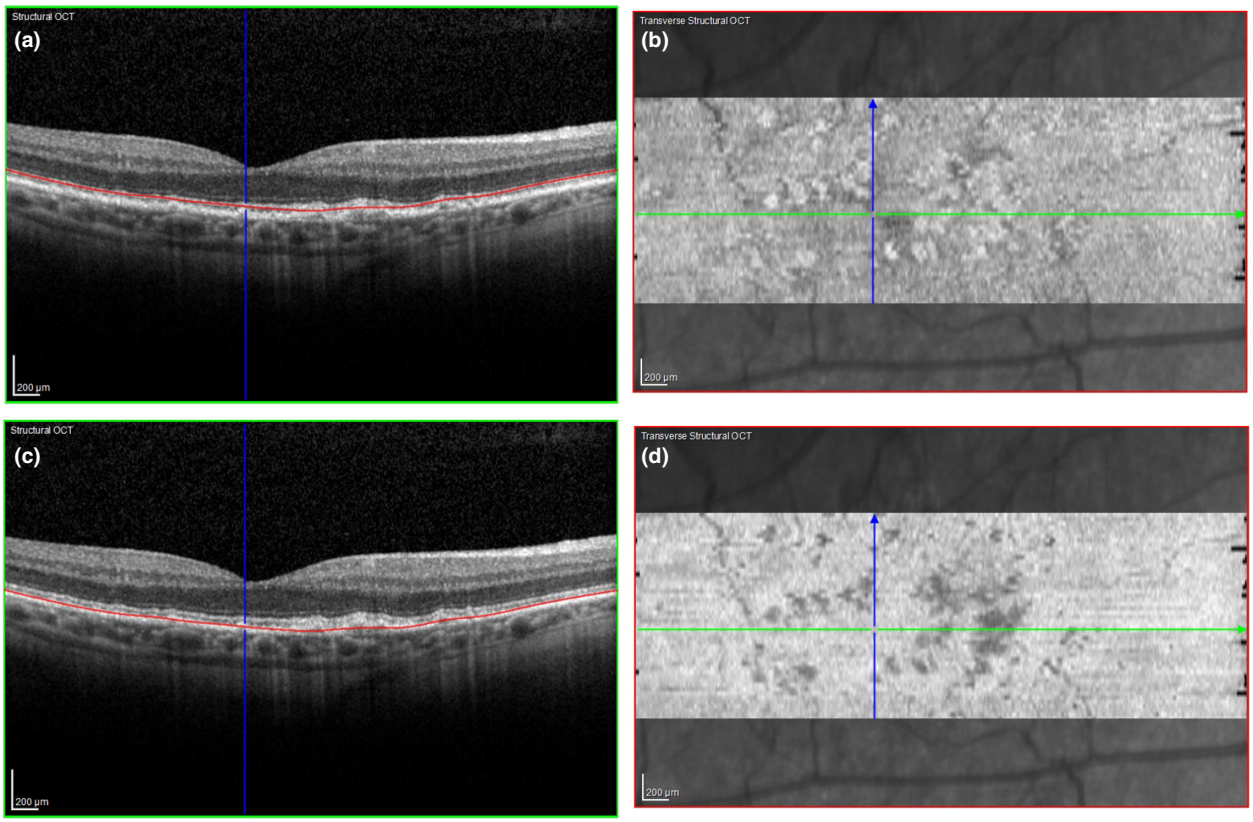


**Figure 4.** Optical coherence tomography (OCT) images of the same subject, 24 years later and prior to exudative age-related macular degeneration (AMD), emphasising that the drusen are larger and more confluent. (a) B-scan at the fovea, with the red line showing the selected superficial border for the *en face* reflectivity computation to show drusen. (b) Slab at the location shown in (a), with the bright spots indicating high reflectivity from drusen. (c) B-scan at the fovea, but with the red line deeper in the fundus. (d) Slab at the location from (c), Showing the deeper regions where the overlying drusen block the light.

strength of a signal between those two layers, displaying drusen (*Figures* 4*c*,*d*) or exudation[50] in an *en face* presentation. This can be accomplished for layers far beneath the overlying and often reflective retina. These OCT segmentation results compare favourably with the multiply scattered light imaging for drusen, although the OCT method requires post-processing and a few seconds of stable eye position. The multiply scattered light imaging method lacks the axial resolution of OCT, but gives nearly instantaneous results in live video or captured images and detects subtle damage that may be missed on OCT.

## Polarisation properties of the human retina: direct backscattered and multiply scattered light and birefringence

Imaging with polarisation provides another way to probe photoreceptors and their microenvironment. Polarised light can be used to provide information similar to confocal imaging and OCT about directly backscattered light from the retina, and can enhance the contrast of retinal blood vessels in healthy eyes and those with AMD or epiretinal membrane.[51–57] Our comparison of an *en face* technique, scanning laser polarimetry, and polarisation sensitive OCT (PS-OCT) demonstrates similar findings for a neovascular membrane in AMD.[57] Light that is directly backscattered retains a high degree of polarisation from the illumination, and many retinal structures act in a manner similar to birefringent crystals.[52,53] The superficial retinal layers that provide strong signals in confocal retinal imaging also are emphasised in the light returning from the fundus that retains polarisation. By acquiring retinal images with varying input polarisation angles, several types of images can be created based on polarisation properties. Computed images can be based on light that retains polarisation, and for which polarisation input angle is varied, but also based on the light that does not vary with polarisation, i.e. is multiply scattered.

The thickness and orientation of regularly spaced axons can be quantified from their polarisation properties, with the cone axons that are a key component of the Henle fibre layer providing a radially symmetric signal at the

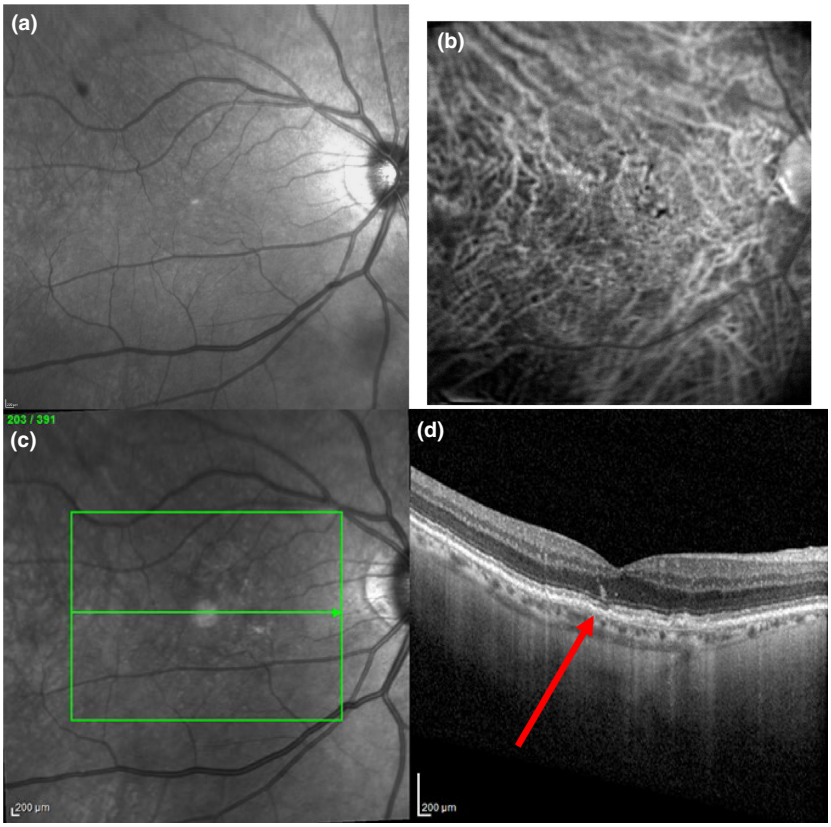


**Figure 5.** Follow-up retinal images of the same subject (a) Confocal scanning laser ophthalmoscope image at 830 nm using the Heidelberg Spectralis, 17 years later, showing the increased size and number of the drusen. There is now an epiretinal membrane, superior temporal from the fovea. (b) Follow-up 28 years after Figure 1 and 6 months after successful treatment for neovascular age-related macular degeneration. Enhancing deeper pathological structures and choroidal vessels with multiply scattered light imaging with red, dual line illumination with the digital light ophthalmoscope (DLO). Unlike the shadows cast by having the illumination to one side, this methods uses symmetric offsets of illumination lines. Sample parameters are 116 µm wide illumination and 0 ± 335 µm offset. The whitish appearance of the optic nerve head is typical for multiply scattered light imaging. (c) Confocal scanning laser ophthalmoscope image at 830 nm using the Heidelberg Spectralis, showing the increased size of the drusen. (d) B-scan through the green horizontal line of the optical coherence tomography data at 870 nm, showing that the drusen are elevated into the outer nuclear layer. Hyperpigmentation is shown as a hyper-reflective band that shows retinal pigment epithelium (RPE) tissue elevated into the outer nuclear layer (red arrow), with adjacent hyper-reflective foci.

fovea known as the macular cross or macular bowtie.[52,53] Imaging with scanning laser polarimetry shows that the macular cross persists in many patients with exudative AMD and is correlated with visual acuity, indicating that cones are still alive.[52,55] The centre of the macular cross also pinpoints the centre of the axons, i.e. the location about which the central cone axons radiate.[58,59] The polarization signal from the Henle fibre layer decreases with increasing age, and also reaches the maximum at a location that increases with increasing ageing,[60] consistent with the previous findings of a decrease of cones in the central most fovea.[61] Thus, again there is evidence for a cone distribution less peaked at the fovea for older subjects. Scanning laser polarimetry reveals a strong signal from scleral collagen in areas of atrophy, with the analysis of the polarisation angle of the maximum signal at each location producing a tessellated pattern, very unlike the radial pattern of the Henle fibre layer signal or the retinal nerve fibre bundles.[52,59]

Depolarised light images, computed from the modulation of the signal from the crossed detector across the polarisation input angles, increase the contrast of drusen and hyperpigmentation, similarly to multiply scattered light images generated when there is no polarisation control.[62,63] Atrophy, exudation, and other pathological features are readily seen in AMD, corresponding to autofluorescence images and angiography.[52,55,64] There is a general increase in multiply scattered light with increased ageing in the foveal region, which has the potential to decrease contrast in vision.[65]

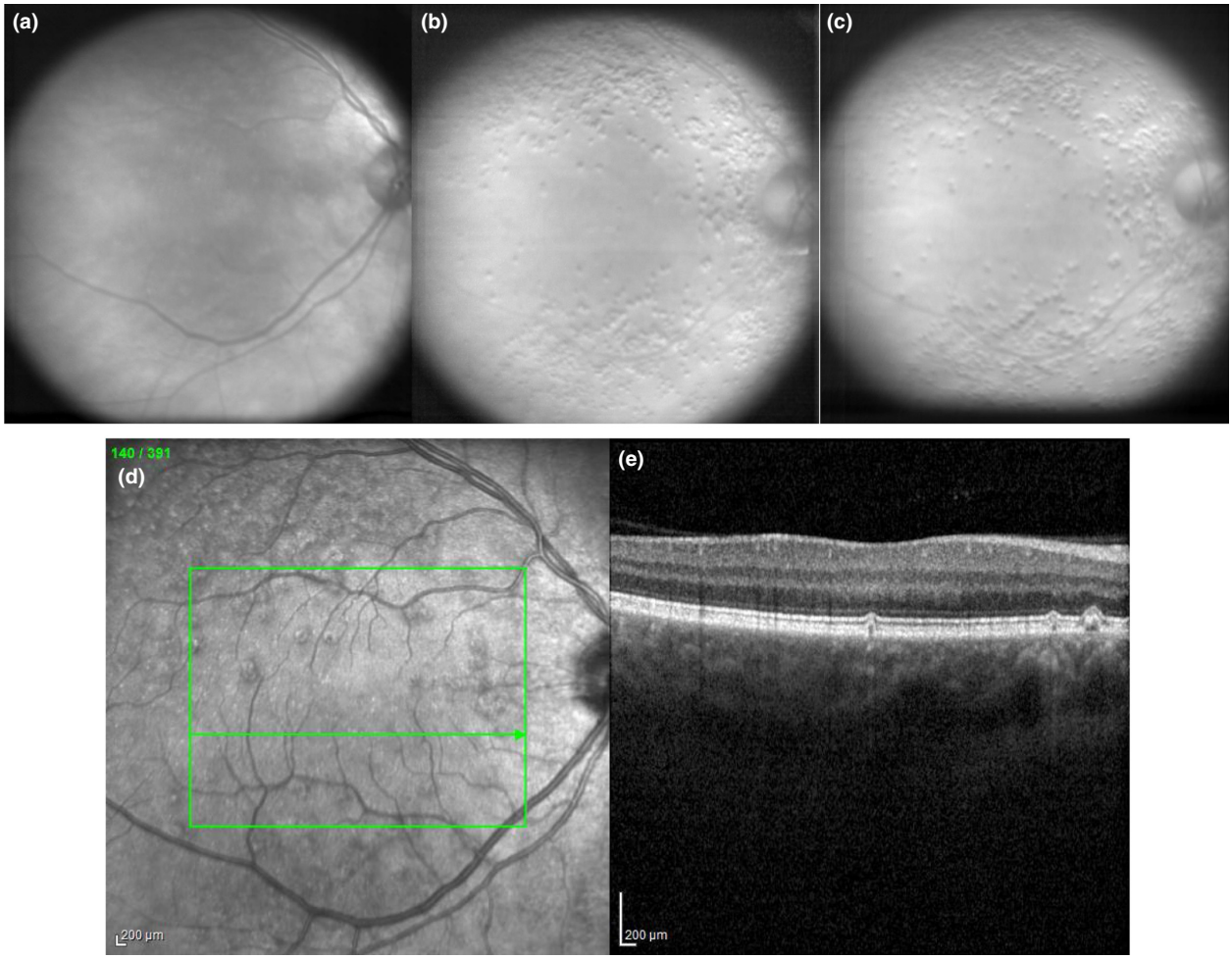


**Figure 6.** Images from a 47 year old female with familial drusen. (a) Confocal image from the digital light ophthalmoscope (DLO). (b) Multiply scattered light image with lagging offset from the DLO, showing drusen that are not primarily in the central macula. (c) Multiply scattered light image with leading offset from the DLO. (Bottom) Spectralis scanning laser ophthalmoscope (SLO) and optical coherence tomography (OCT) B-scan (d) SLO imaging of same patient, again showing the familial drusen that are not primarily in the central macula. (e) OCT B-scan, at the location of the green line in (d), showing the depth and thickness of drusen.

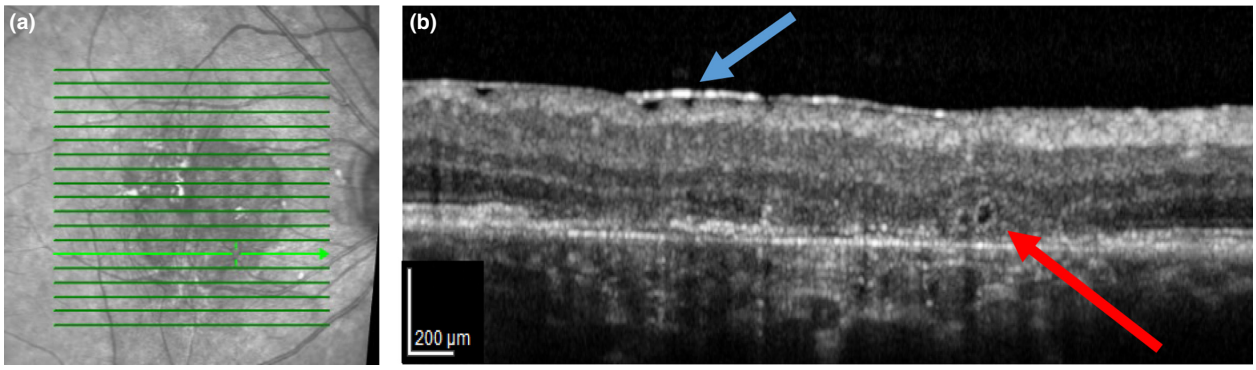


**Figure 7.** Outer retinal tubulation (ORT) in an 80 year old subject with non-exudative age-related macular degeneration (AMD) (a) Scanning laser ophthalmoscope (SLO) image, with green scan line for location of the ORT. (b) The corresponding optical coherence tomography (OCT) image, with adjacent ORTs (red arrow) and the overlying epiretinal membrane. Adapted from King *et al*.[49]

## Function and physiology measurements

Mapping the physiology over time for both photoreceptors and their microenvironment, particularly blood vessels, is advancing rapidly. Wide field techniques using the SLO map the photopigment density across the retina by measuring the logarithm of the difference between the reflectance of the dark adapted vs bleached retina, using a wavelength that has high absorption for the photopigment of interest.[21,23] For cones measured with 594 nm light, there is decreased optical density of photopigment in the foveas of older eyes.[61] In the same subjects, macular pigment is correspondingly decreased, measured by using 488 and 514 nm in the bleached retina. Decreased photopigment is consistent with decreased density of cones, decreased photopigment or outer segment length for each cone, or both. There is an extreme decrease of photopigment in the fovea with AMD (*Figure* 8). These results are consistent with the psychophysical technique of colour matching, in which the optical density is measured as a function of light level as the photopigment is bleached with bright lights.[66–68] The decreases in photopigment for these patients with AMD occur despite visual acuity sufficient to constrain it to be subserved by the densely packed cones in the fovea. These findings indicate that there are several cones remaining in their foveas, surviving over decades, but having either shortened outer segments or less photopigment per cone. That is, cones are maintained but with a more economical configuration such as lower photopigment density or not maintaining the normal increased cone density from the periphery to nearer the fovea (*Figure* 9), two potential aspects of the neural economy hypothesis.

The comparison of structure and function directly at comparable locations, such as mapping the light sensitivity or other types of visual function, can be accomplished by providing a target, such as a flash of light at a known retinal location that is coplanar with a live image of the retina from an SLO.[69] As the targets are typically presented in Maxwellian view and with a small exit pupil, variation in intensity and other effects due to pupil size variations across subjects are minimised. While microperimetry or fundus perimetry are the best-known applications, there are two broad types of methods for functional measurements, as detailed previously.[35] One method includes projecting the stimuli or the stimulation beam onto the retina with one or more of the same beams used for imaging the fundus.[69] The stimulus can often be observed directly on the fundus, without the need for calibration of the stimulus position to the image. The other method uses a stimulus or stimulation method that differs from that used to image the fundus, with stimuli produced readily using a light emitting diode, liquid crystal display, or digital light projector.[18,19,35,70–72] The stimulus channel is then combined with and calibrated to the imaging channel. Another variation in method is whether the stimulus is tracked with a goal of stabilisation of the stimulus position on the retina vs the registration of the stimulus to the retinal location via post-processing of images. When near NIR light is used for illumination, it becomes unnecessary to use bright targets or decremental targets to allow detection over a bright illumination field.[18,19,35,70–72]

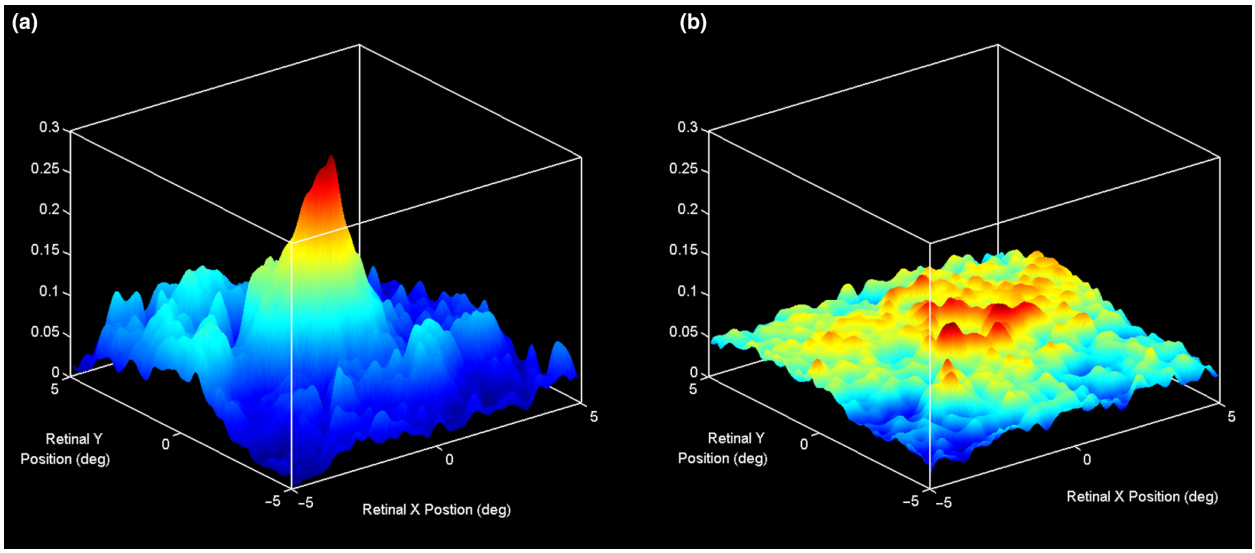


**Figure 8.** 3-D maps of cone photopigment density difference at 594 nm with a scanning laser ophthalmoscope (SLO), using reflectometry. (a) Normal 22 year old subject, showing a high peak and steep drop-off of cone photopigment at the fovea. (b) Patient with age-related macular degeneration (AMD), showing a low and uneven density of photopigment. Adapted from Elsner *et al.*[61]

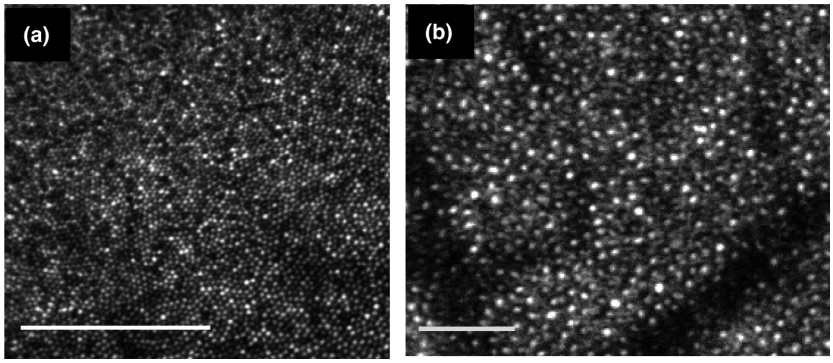


**Figure 9.** Cones of a 34 year old male with a normal retina, as seen on adaptive optics scanning laser ophthalmoscope (AOSLO). (a) Foveal sample, with the fovea in the upper left of the image, showing densely packed cones and a regular array without rods or other large structures in plane. Note both bright and relatively isolated dark cones in the array. (b) Cones at 10 deg temporal retina, showing a regular array of cones, but larger and more widely spaced. Between cones are rods and presumed teleodendrites, which appear as fibrils, demonstrating the more varied structure in this plane at eccentricities outside of the foveal region. Scale bars = 50 μm. Adapted from Burns *et al*.[33]

The comparison of structure and function has included specific fundus lesions or types of pathological changes, with sensitivity compared with control regions or control subjects. Relatively decreased sensitivity is associated with hyperpigmentation in high myopes.[72] Similarly, decreased sensitivity is spatially associated with drusen and hyperpigmentation, and particularly atrophy and exudation, in AMD.[73] Nevertheless, while there is loss of sensitivity, there can be some sensitivity at or near these key features of damage in AMD. Further, patients with AMD can use small clusters of fixation locations, even when these are adjacent to geographic atrophy.[35]

Comparison of structure and function can better determine the sources of variability or decrease of sensitivity near the optic nerve head. Mapping the blind spot has unique issues, in that the optic nerve head may be tilted (*Figures* 10*a,b*) to the extent that the highly reflective superficial tissues mask the location of the scleral rim (*Figure* 10*b*). Details of the optic nerve head and the scleral crescent are often readily visualised in NIR light (*Figure* 3),[17] but less well visualised with ophthalmoscopy or flood illuminated fundus photography. This leads to variability when comparing structure and function. By using multiply scattered light, the choroidal rim of the optic nerve head can be better visualised (*Figures* 3*b and* 10*c*).

## Methods for mapping the blind spot and results concerning variability

Mapping the blind spot while viewing the fundus has improved our understanding of structure and function.[35] Using a laser scanning digital camera equipped with a digital light projector to provide visual stimuli,[35] we projected a 0.5 deg, white, incremental target for kinetic perimetry. We mapped 12 meridians radiating out from the centre of the optic nerve head, measuring two trials each of 'seen to not seen' and of 'not seen to seen.' Fixation to a red, 0.5 deg circle was monitored, and images were captured at 12 Hz with NIR imaging in a 35 × 35 deg field of view. The highest myope in a series of three adult (25 ± 6 years) subjects had a spherical equivalent of −7.75 D and an axial length of 26.17 mm (IOL Master, Zeiss, www.zeiss.com). The disc was tilted on OCT (*Figure* 10*a*), with projection into deeper layers of the light not absorbed, i.e. where the RPE was missing, the deeper layers had areas of increased intensity, consistent with the confocal *en face* images (*Figures* 10*b–d*). The scleral crescent was greatly enlarged and contained clumped hyperpigmentation within a wide area where there was no pigmented RPE (*Figure* 10). The multiply scattered light image similarly demonstrated that the scleral crescent area did not return light where there was no RPE, and that the apparent edge of the optic nerve head did not match with the choroidal rim (*Figure* 10*c*).

Kinetic perimetry includes a delay according to the criterion of a subject, which may alter the location reported that they first see the target or no longer see the target. This delay leads to variability across subjects (*Figure*10*d* vs 10*e*), but the highly myopic subject responded on both trials as 'seen' over the specific region of peripapillary atrophy (*Figure* 10*d*). These results suggest that there may be cones in the peripapillary region, but there also could have been a response from scattered light for the target falling onto healthier retinal regions.

Another issue in assessing function near the optic nerve head is that many perimetry paradigms use brighter targets on a dimmer background, with potential false positive responses based on target light scattering onto more normal tissue. We found that darker targets on bright background led to smaller blindspots.[35] Using a DLO with stimuli produced by extinguishing the imaging illumination at the

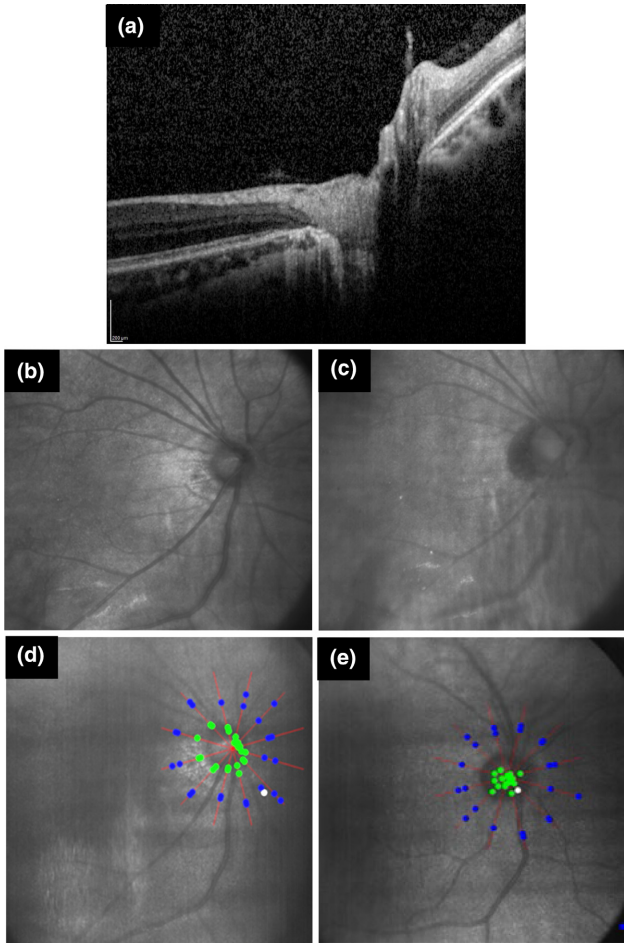


**Figure 10.** Potential sources for variability of sensitivity in the peripapillary region (a) Optical coherence tomography (OCT) B-scan of the myopic disc of a right eye, showing a tilt disc and peripapillary atrophy and hyperpigmention. The photoreceptor layers within the peripapillary zones are irregular, indistinct in locations that correspond to the large scleral crescent in (b) and (c), and also consistent with the variable projection of light into the deeper fundus layers where there is no pigmented retinal pigment epithelium (RPE). (b) Infrared confocal image of the large scleral crescent of a myopic adult, with a digital light ophthalmoscope (DLO), showing the large area of peripapillary atrophy with clumped hyperpigmentation in a myopic subject. (c) Multiply scattered light image of the same peripapillary region. The choroidal rim in (c) is not readily located from the confocal image in (b). (d) DLO mapping of the blind spot using kinetic perimetry with Goldmann III white targets on a dimmer white background. The green circles indicate 'seen to not seen' and the blue circles 'not seen to seen.' At 9 o'clock, the blue circles indicate that targets are 'seen' that did not travel over any region with pigmented RPE. This indicates that there was a response from light within or neared to the scleral crescent. At other locations, e.g. 7, 10, or 11 o'clock, the target has travelled over a region with RPE. (e) Corresponding map of the blind spot for an emmetropic adult, who lacks peripapillary atrophy or hyperpigmentation. The blue circles, indicating 'seen' at the 9 o'clock position are fairly similar from the centre of the optic nerve head as compared to the other meridians, with the target travelling over a similar amount of pigmented RPE before being detected, (f) Imaging of mapping the blind spot for an emmetropic eye with a large scleral crescent, but using the DLO to project a dark target. Retinal image of a Goldman V, kinetic target on a brighter red background. The dark spot at 3 o'clock on the scleral crescent is the actual target projected onto the retina, indicating detection within the scleral crescent at this location. (g) Full map of the blind spot, as indicated by red circles, of the subject in (f), showing five of eight seen locations falling on or partially on the scleral crescent. (h) Adaptive optics scanning laser ophthalmoscope (AOSLO) images of cones in the peripapillary crescent of a myopic subject. Arrows indicate (1) the edge of the crescent, (2) the edge of the optic nerve head, and (3) the opposite edge of the optic nerve head. (i) The area within the box in panel (h), with the arrow marked as 1 showing cones on the depigmentated crescent, where the RPE has pulled away. (j) Enlargement of the area within the box in panel (i). Adapted from Chui *et al.*, 2012.[82]

target location, we mapped the blindspot with dark targets in 12 undilated adults, 25–63 years. Confocal retinal imaging was performed at 20 Hz with a 35 deg field of view. The imaging and background illumination was provided by a red 630 nm LED, with 40 μW time-averaged power at the cornea. We continuously captured images of the dark target projected onto the retina, showing when the subject responded (*Figure* 10*f*). We observed positive responses in a

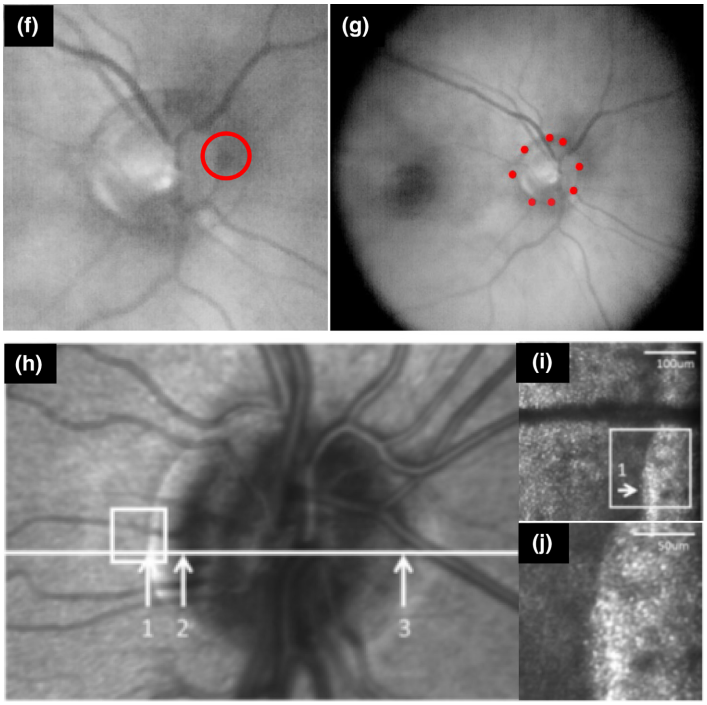


**Figure 10.** (Continued).

rare normal subject who had a wide enough scleral crescent to fit a Goldmann V stimulus (*Figures* 10*f,g*). These results suggest that there are cones along or within the scleral crescent, and the results cannot be attributed to long range scattering onto normal retina. These cones may have decreased sensitivity due to their orientation or lack of normal RPE, as discussed in more detail below, but may contribute to the detection of targets. This suggests that blind spot mapping may not actually provide the most accurate size of the optic nerve head.

A variety of imaging techniques have been used to map and quantify retinal and choroidal vessels, many using the changes in signal over time due to blood flow. While earlier SLO techniques used contrast agents such as sodium fluorescein and indocyanine green to map and quantify perifoveal intercapillary area, the avascular zone, retinal lesions such as microanurysms, as well as otherwise difficult to detect subretinal exudation that is masked by overlying retinal pigments or blood.[25,41,52,74–76] The use of barrier filters in angiography, along with the excellent signal-to-noise ratio that is available in an SLO, led to the detection of weak signals from autofluorescence of the RPE and degrading exudation.[25]

The motion of red and white blood cells through the smaller retinal blood vessels have long been known to allow blue field entoscopy, so that a subject can trace the foveal avascular zone and surrounding vessels by the detecting changing pattern of the transmission of short wavelength light for white blood cells that is interspersed with shadows from red blood cells. This pattern matches the foveal avascular zone measured with fluorescein angiography on SLO.[75] Observing the blood flow through the retina and choroid with an SLO has facilitated the documentation of vascular remodelling in retinal diseases, such as AMD, that demonstrates the extreme environment of cones when a retinal-retinal anastomosis, tangles of retinal vessels, or leakage develop beyond just choroidal neovascularisation.[43] These vascular lesions, therefore, span between the layers beneath the photoreceptors to layers above, totally altering the microenvironment of photoreceptors. While these complexes were originally called retinal vascular anomalous complex[43] they are now known by other names such as retinal angiomatous proliferation (RAP).

A variety of imaging methods that use temporal variations document the relative lack of oxygen available to support photoreceptors. Laser Doppler flowmetery demonstrated that there is less choroidal blood flow in older eyes compared with younger ones, and similarly less choroidal blood flow on average in eyes with AMD compared with age-matched controls.[77] A complementary finding of decreased blood flow in a patient with AMD, compared with controls, was concluded from the temporal variation a line-scan SLO and measured using image stabilisation.[34] The Laser Doppler method used a safe light level of a 670 nm laser and the line-scan SLO used NIR illumination, indicating that blood flow measurements to

document potential hypoxia of photoreceptors can be safe and comfortable for the patient.

## Adaptive optics

To improve imaging of retinal structures, modern high magnification imaging devices have enough signal to noise ratio at safe levels of light, but the aberrations of the human eye must be overcome.[33] However, high resolution retinal images require the imaging instrument to have a high numerical aperture, which means a large pupil size. The aberrations that vary with pupil position degrade image quality. Cones outside the centralmost fovea can nevertheless be imaged in eyes with good optics, since cones guide the light both into the retina and back to the imaging instrument.[78] Again, image contrast is improved when using laser scanning and confocal apertures. However, for the highest density cones and many other structures, only by correcting aberrations across the pupil can the contrast improve sufficiently to visualise small or subtle structures.[33] For instance, normal retinal capillaries could finally be visualised without the addition of a contrast agent such as sodium fluorescein, when using a phase plate at the pupil plane to correct aberrations in a SLO instrument.[79] A variety of methods are now used for computing and/or measuring wavefront aberrations and compensating for these aberrations, frequently in real time by using adaptive optics (AO), such as a deformable mirror, and are reviewed in detail.[33] The resulting instrument is an adaptive optics scanning laser ophthalmoscope (AOSLO), although AO instruments using flood illumination can provide high speed imaging, but at the cost of contrast.[33] Not only are cones readily visualised with AOSLO, but also unexpected remodelling of retinal microvaculature has been demonstrated.[80]

A variety of functional measurements is possible on a microscopic scale using AO, with the potential to map the location of the stimuli with respect to the retina, also reviewed in detail.[33] As with the wider field stimuli, there are two main types of methods for functional measurements. One method includes projecting the stimuli or the stimulation beam onto the retina with one or more of the same beams used for imaging the fundus. The other method uses a stimulus or stimulation method that differs from that used to image the fundus, such as in wavelength range or resolution. The stimulus channel is then combined with and calibrated to the imaging channel. Another difference is, as with wider field fundus perimetry, whether the stimulus is tracked with a goal of stabilisation of a stimulus on the retina vs registered to the retinal location via post-processing.

The density of cones in normal and diseased maculas has received considerable attention from many laboratories.[33] The density of cones has long been known to be greatest in normal eyes in the fovea, and then decreases rapidly with increasing retinal eccentricity (*Figure* 9), but large individual variations made comparison to diseased eyes difficult.[81] The shape of the cone density distribution is consistent with the above findings from retinal densitometry, a sharp peak of cone density in the foveas of young subjects, and a steep falloff with increasing eccentricity, but a flatter function and often lower densities in many older subjects (*Figure* 8).[67]

In addition to eccentricity, meridian and refractive error are related to the large individual differences in the distribution of cone density.[47,82,83] Cone density is higher in the nasal and temporal meridians than the superior and inferior meridians, although near the optic nerve head the distribution is no longer smooth.

For a set of 36 healthy subjects <35 years of age and with axial length <26 mm, the distribution of cone density is well-fit by a two parameter model,[81] using the natural logarithm (ln):

$$\ln(\text{cone density at } x \text{ eccentricity in microns}) = a + b * \text{eccentricity in microns}$$

The main two factors are (1) overall cone density and (2) change in density with eccentricity, which is the result of developmental cone migration.[15] From this model and computing the expected ratio of cones for temporal, nasal, superior, and inferior meridians, several computations are possible. Using data of only two locations that differ in eccentricity and are far enough apart, it becomes possible to calculate the total cones in the central 14 deg of the macula, or to estimate cone density at any retinal location within this area for young, normal subjects.

The data and this model reject the idea that all subjects have an equal number of cones in the central macula, although the variation of total cones in the central 14 deg is less across subjects than the variation at any given retinal location. Also, the variation of cones near the central fovea is larger than for any other location.

The neural economy hypothesis predicts that older eyes, assuming decreased support of the microenvironment, would have fewer cones. Cone density decreases on average with increasing age, but there is considerable overlap between younger and older subjects.[47,83] As stated above, the ONL is thicker in the older subject group, rather than thinner, which would be expected if there were no structural changes other than loss of photoreceptor cell bodies. The thickened ONL is consistent with remodelling and Müller cell changes.[84] For older subjects, the ratios of cones for temporal, nasal, superior, and inferior meridians are less closely related to each other or that of the younger subjects.[47] Thus, the confidence limits become larger for older

subjects. One possible reason is that the decrease in cone density with ageing may represent an overall loss of cones, migration back outward following vitreous detachment, or changes with other aspects of the ageing microenvironment that allow a decrease of cones. These complex factors have not yet been captured in a quantitative model. Further, specific locations, such as near the optic nerve head, may favour cone survivability.[85]

Myopes have cone density distributions that reflect, among other factors, retinal stretch and slip. In healthy but myopic eyes, there is often an increase in axial length that pulls the RPE away from the underlying retina in the peripapillary region, which changes the usual optical properties of the photoreceptor/RPE complex (*Figure* 10).[82] The peripapillary crescent is readily identified by the lighter appearance, due to decreased melanin absorption over the scleral collagen. The cones do not have the usual appearance of the densely packed ones that are farther from the optic nerve head, and instead appear sideways and are disarrayed rather than packed hexagonally.

The fact that cones survive without RPE in the peripapillary regions of young adult myopes may help explain our finding of the survival of sick cones for years in patients with AMD.[82] Further, some cones survive within ORT, where there is extensive remodelling of the retina and RPE, often with missing RPE and various presentations of atrophy (*Figure* 11).[49] Using AOSLO, cones in areas of RPE atrophy have been shown to guide light in confocal mode,[49] and cone cell bodies are quantified as the bumps in degenerating retinas by using multiply scattered light mode.[49,86] In the healthy eye of a young adult, cone density is evenly distributed without disruptions, other than the decrease with eccentricity or changes at the optic nerve head, even several degrees outside the fovea (*Figures* 8 and 9).

The Indiana AOSLO instruments have been optimised for ageing eyes rather than the highest possible resolution.[33] Thus, while diffraction limited imaging is available, images are routinely acquired with a pupil diameter smaller than 8 mm, i.e. a less than optimal numerical aperture. There is also custom software that removes the signal for AO correction from regions of the pupil with poor transmission, such as from cataract.[87] This method reduces signal, but reduces noise, so that the overall signal to noise ratio is better. Further, the confocal aperture used for imaging cones is variable, often 2 Airy disc diameters in the emmetropic eye, although images could be obtained with smaller apertures but have weaker signals. These are two of the many design characteristics that make imaging in older eyes robust. The optical degradation is still present from poor tear film, scatter within older lenses, and poor fixation due to fatigue and especially with central vision loss. The unsteady fixation is partially compensated by montaging all the individual images, which corrects the position although

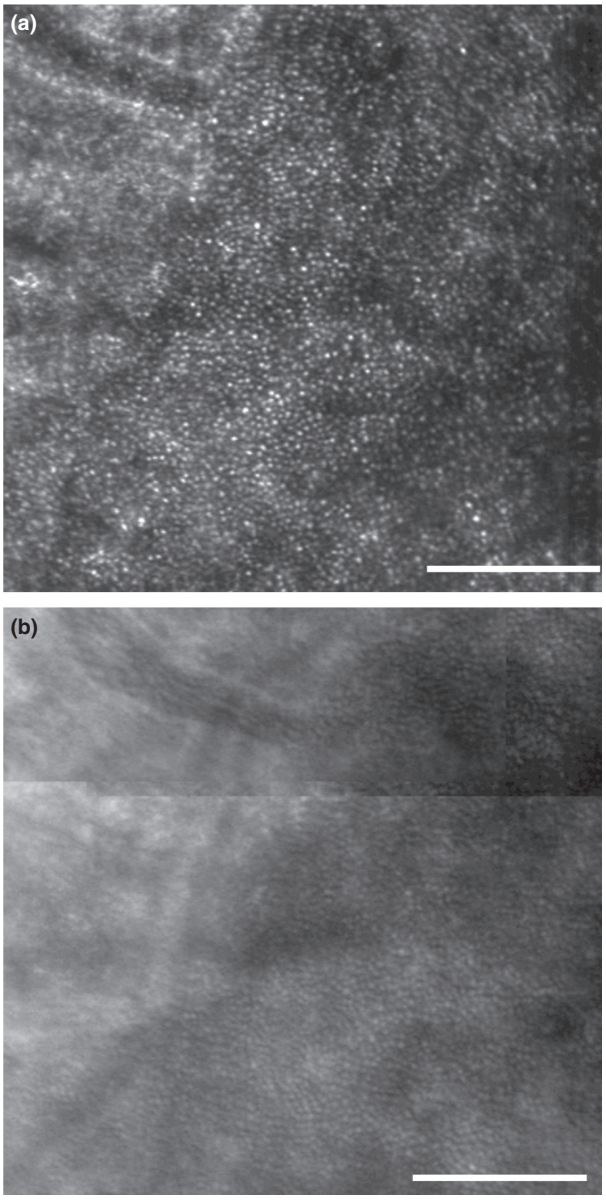


**Figure 11.** Adaptive optics scanning laser ophthalmoscope (AOSLO) imaging of the border of an atrophic region of retina in a 56 year old subject with rod-cone dystrophy. Within the atrophy, there is a long outer retinal tubulation (ORT) bridging it, and several smaller ORT running from a less abnormal region of retina into the atrophic region. (a) Confocal image, showing cones guiding light. There are densely packed cones outside the region of atrophy on the right and bottom, and cones that are seen as oriented sideways along the ORT, with sparse cones elsewhere including within the atrophy. (b) Multiply scattered light image showing the corresponding view that appears more three dimensional. The inner segments of cones are packed densely at the right and bottom. Elongated structures are seen on the ORT, where there are cones guiding light in the confocal view. There are bumps corresponding to the foci of cones guiding light in the confocal view. Scale Bars = 200 μm. Adapted from King *et al*.[49]

not motion artefact (*Figure* 11). These AOSLO features permit the measurement of cones that may have weak guiding.

## Changes over time producing blood cell motion mapping with AOSLO and OCTA

The metabolic support from retinal and choroidal vessels is important for both neural and glial retinal structures, and is a key component of the microenvironment of cones. When there is metabolic disturbance and when the RPE does not function normally, the dependence on retinal vascular support might increase. This may explain part of the finding that anti- vascular endothelial growth factor (VEGF) therapy can increase GA,[88] i.e. the choriocapillaris is already compromised and the anti-VEGF further reduces choroidal and retinal circulation. Not only is metabolic support important, but also RPE pumping of retinal fluid, which can exit the choriocapillaris when it is intact. With the break-down of the RPE tight junctions and insufficient pumping, the fluid can remain in contact with the photoreceptor outer segments. We found that cones may not guide light normally in patients with diabetes, i.e. they are present but dark, likely due to excess fluid that can be visualised in some patients on OCT.[89] Fluid transport via Müller cells is an alternative mechanism of balancing and removing fluid and ions,[30] which may become taxed when the RPE fails in these roles. The retinal circulation may then play an even larger role in maintaining ionic and fluid balances for retinal neurons of the cone pathways.

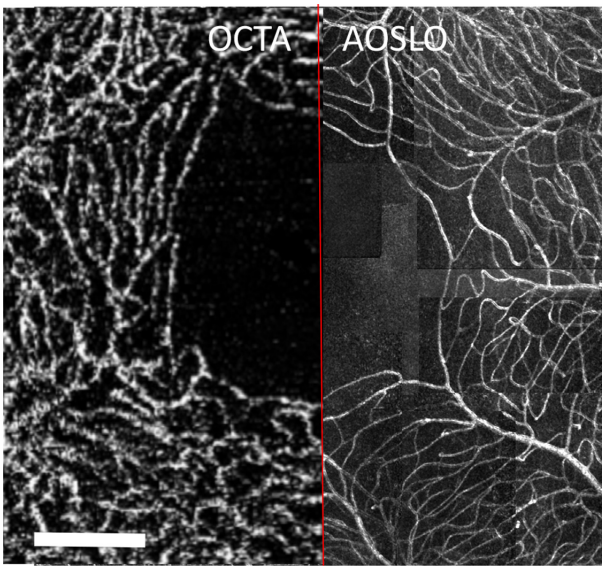


**Figure 12.** Mapping of the superficial vascular plexus around the foveal avascular zone (FAZ) of a 27 year old normal male, using motion mapping or the local change over time of red blood cells. Left side- Optical coherence tomography (OCTA). Right side- Adaptive optics scanning laser ophthalmoscope (AOSLO). Adapted from Burns *et al.*, 2018. Scale bar = 200 μm. Adapted from Burns *et al.*[33]

Maps of the retinal vasculature can be made by computing the change over time of the light returning from the retina, using either the OCT angiography signals (OCTA) or the AOSLO signals (*Figure* 12). The OCTA maps are depth resolved, capable of separation of three capillary plexus maps,[90] with projection of forward light scatter or shadowing from dense overlying structures still undergoing software improvements. For diseases such as diabetic retinopathy[31] and AMD with geographic atrophy,[30,91] the pathological changes to the retina can be visualised in different layers, although subject to segmentation artefacts for highly distorted retinas. For AOSLO motion maps, there is much better lateral resolution, and the potential to separate out the main capillary plexuses, but much smaller field sizes.[31,33,80] The choriocapillaris is less well resolved on AOSLO and on OCTA, although individual capillaries are not well-visualised. Direction of flow is visualised with video from reflectance images. The images from either technique can be montaged to provide a larger field of view,[31,33,80] and have the potential to agree well when the lower lateral resolution of OCTA does not combine or miss small vessel changes. OCTA and AOSLO vascular maps provide a wide variety of outcome measures for assessing the metabolic support available from the various vascular levels, e.g. capillary density, pores between capillaries, peri-arteriole and peri-venule capillary free zones, foveal avascular zone acircularity, etc.

## Methods for probing the cone microenvironment with the DLO

To probe variations of the cone microenvironment corresponding to the deeper fundus layers, we recruited 16 subjects with a broad variety of ocular health, from normal to exudative AMD. All had at least one eye without exudative AMD. Subjects ranged in age from 26 to 68 years, (mean 47 years, S.D. 14 years). The study adhered to the tenets of the Declaration of Helsinki, and informed consent from all subjects was obtained prior to experimental data collection. The study was approved by the Indiana University Institutional Review Board (IRB).

Nonmydriatic confocal and multiply scattered light images were acquired with a DLO,[36,37] which uses a Digital Light Projector (DLP™) (Texas Instruments, www.ti.com) as a light source, described previously.[37] The DLP™ presents a series of projected line patterns swept across the retina, instead of mechanically scanning a laser. For NIR

imaging, one or more line patterns of a custom module with a 860-nm illumination vertical cavity surface emitting laser (VCSEL) were projected sequentially to form a 28 deg raster. For visible wavelength imaging, the LEDs supplied with the DLP were filtered as follows: red (630 ± 10 nm) and yellow (570 ± 20 nm). Both light sources minimised unwanted speckle in the images.

Detection is performed using a complemenrtary metal-oxide-semiconductor (CMOS) rolling shutter to read sequentially only those in synchronisation with the illumination lines, providing an electronic rolling shutter as described previously.[35–37] When sampling at 1024 × 1024 pixels for 38 and 28 deg, the digital resolution was nominally 11.1 and 8.2 μm/pixel, respectively, for an emmetropic eye. While this resolution is inadequate to visualise foveal photoreceptors, it is more than sufficient to image drusen, RPE hyperpigmentation, and blood vessels that have sufficient contrast from their background.

Confocal imaging occurs when the sufficiently narrow illumination lines are projected in synchrony and on-axis with the lines detected. Multiply scattered light imaging is performed by shifting when the detection occurs with respect to the illumination, e.g. the detection aperture is electronic and can vary in width as well as the detection timing offset with respect to the illumination. For both NIR and red imaging, a leading and a lagging illumination line were used in sequential image sets. Pairs of leading and lagging offsets were used to observe the shadows of scattering defects cast in opposite directions (*Figure* 13). For red imaging, two illumination lines were used, symmetric about the location of the lines detected, to create multiply scattered light images without a shadow on one side or the other of features (*Figures* 6*b,c* and 13*b,c*).

Subjects were also imaged with SLO (830 nm) and OCT2 (Spectralis, www.heidelbergengineering.com) contemporaneously and for the same eye. Dense (11 μm) B-scans were acquired over 20 × 15 deg. An ophthalmologist graded the OCT B-scans for drusen and other lesions, and then reviewed the DLO images and OCT images for congruency and size (Photoshop, www.adobe.com).

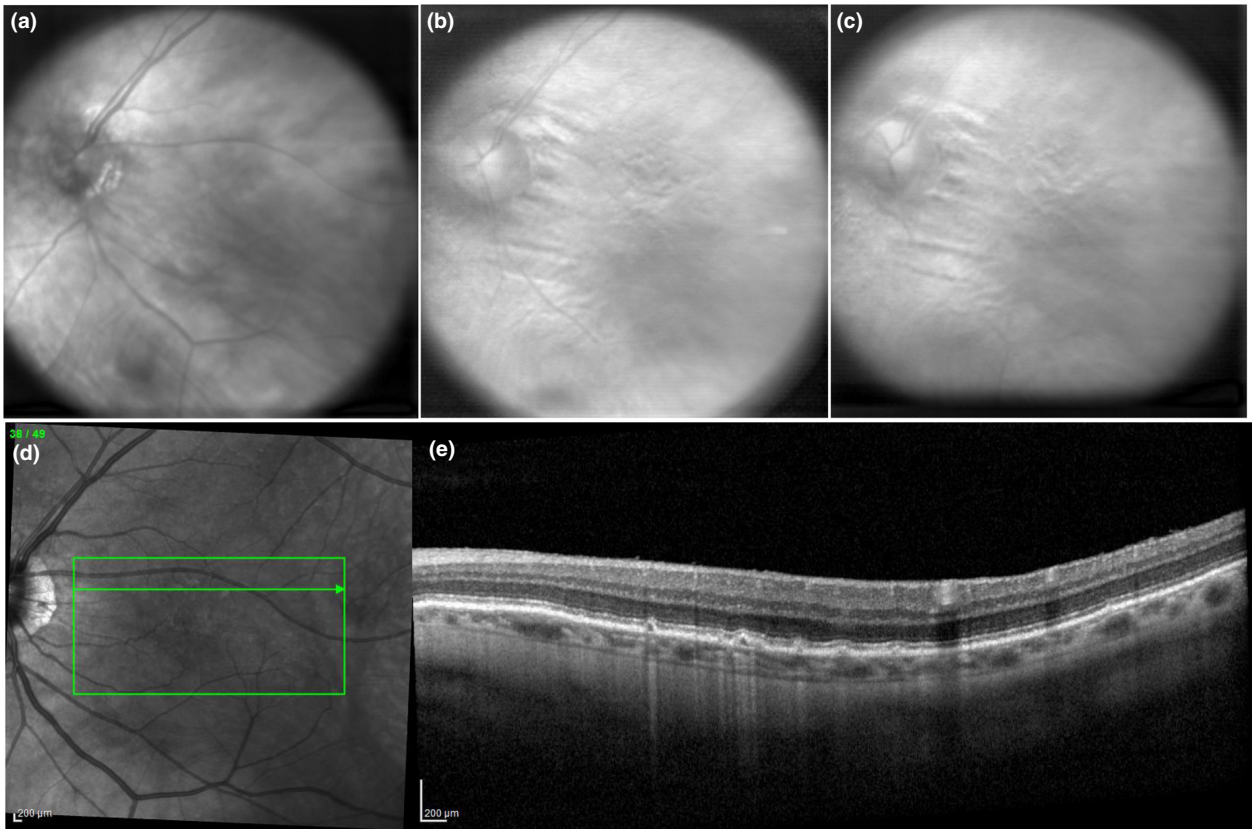


**Figure 13.** Images from a 68 year old male with age-related macular degeneration (AMD), comparing digital light ophthalmoscope (DLO) with optical coherence tomography (OCT). (a) Confocal image from the DLO. (b) Lagging offset multiply scattered light image from the DLO. (c) Leading offset multiply scattered light image from the DLO. Between the fovea and optic nerve head is a region of traction from an epiretinal membrane, seen as striae. (d) Spectralis scanning laser ophthalmoscope (SLO) retinal image of the same eye. (e) OCT B-scan through the green line inside the green box, showing drusen that are visualised as bumps in panels (a) and (b).

## Results of probing the cone microenvironment with the DLO

Five of the 16 subjects had drusen and other lesions identified with OCT (*Figures* 6 and 13). Three of these subjects had 10 total lesions seen on OCT but not on the Spectralis SLO, and 8 of these 10 lesions were identifiable in the DLO multiply scattered light images. The two lesions not identifiable within the multiply scattered light images were very small, having diameters of approximately 23.5 and 25 μm, and were associated with defects within the photoreceptor layers only. All drusen identified with the OCT B-scans were identifiable in the DLO multiply scattered light images, even when the lesions had a thickness of only 12 μm.

A large number of lesions were visible in two subjects on SLO and OCT, which were identifiable on the DLO multiply scattered light images (*Figures* 6 and 13). The drusen in the DLO multiply scattered light images were conspicuous by their cast shadows, which were in opposite directions for leading and lagging aperture offsets. Regions of confluent drusen had shadows cast at the edges rather than for individual drusen (*Figure* 13*b,c*). Thus, these methods, along with previously used variants, detect and localise drusen and other deposited debris beneath the photoreceptors. This documents reduction of the quality of the microenvironment for cones, since there is a partial barrier to the transport nutrients and waste products for the overlying photoreceptors. As these deposits develop over decades, the cones likewise have decades to adapt to this poorer microenvironment.

## Methods for cone imaging and quantification

To document cones surviving without normal RPE using AOSLO, we selected two types of subjects. First, to document cones living without RPE but in eyes without additional changes to the microenvironment that are caused by high myopia, glaucoma, AMD, or other disease, we recruited two subjects with healthy eyes, but unusually large peripapillary crescents. Unlike our previous study in myopes that showed cones surviving in the large peripapillary crescents due to axial elongation causing the RPE to slip away from beneath the retina, these subjects did not have high myopia. Both subjects met our criteria for normal subjects: axial length <26 mm and <3D of spherical error.[81] The width of the scleral crescents was narrow compared with that of most of the myopes that we have studied, but wide enough to permit some visualisation of cones, if present (*Figure* 14).

Second, to document whether cones living in atrophy in AMD was a general finding, or occurred in only select patients or in the presence of ORT, we recruited five patients (two males, three females) with AMD and at least one area of geographic atrophy in the macula as seen clinically and as a transmission defect on OCT due to the missing RPE melanin. Mean age was 75.2 ± 6.11 years. Visual acuity ranged from 6/9 (20/30) + 2 to 6/15 (20/50) in the eye of test, indicating that one or more island of functioning cones existed.

The study adhered to the tenets of the Declaration of Helsinki, and informed consent from all subjects were obtained prior to experimental data collection. The study was approved by the Indiana University Institutional Review Board (IRB).

All subjects were imaged using the AOSLO and NIR light, as previously described,[81,83] to quantify cones using both confocal and multiply scattered light imaging. Data were processed with custom software following data collection. The subjects with healthy eyes but large peripapillary

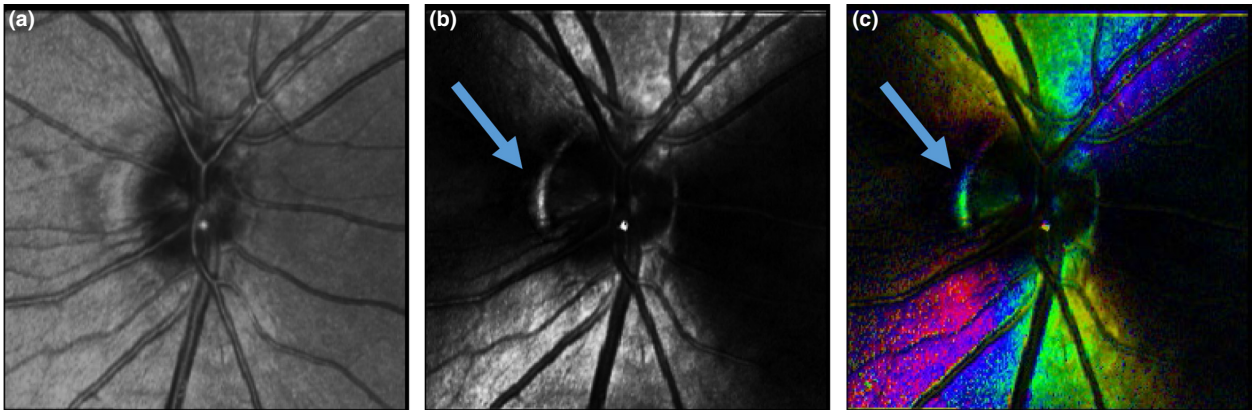


**Figure 14.** Scleral crescent of low myope with birefringence from confocal scanning laser polarimetry. (a) Confocal image. (b) Birefringence in grayscale, with white indicating more phase retardance, revealing the scleral crescent where the retinal pigment epithelium (RPE) is pulled away (blue arrow). (c) Pseudocolor birefringence image, colour coded according to the polarisation input angle leading to the maximum signal, showing the retardance due to the retinal nerve fibre bundles and the variation due to the scleral crescent (blue arrow).

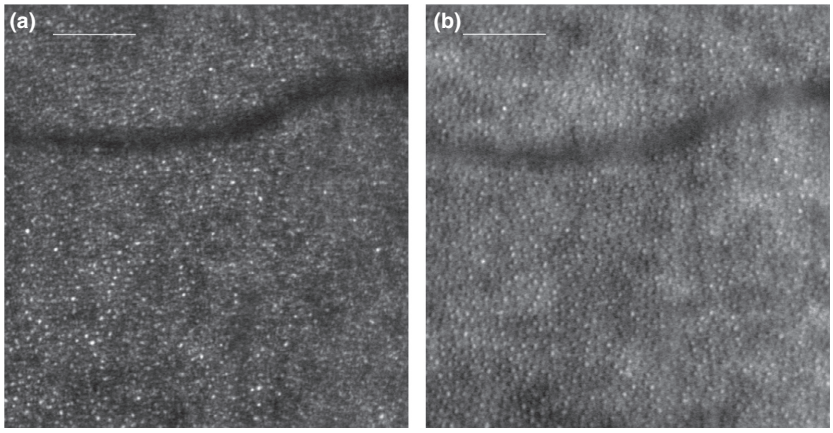


**Figure 15.** Cones just temporal to the optic nerve head in an emmetrope with adaptive optics scanning laser ophthalmoscope (AOSLO), showing similar density, size, and orientation of cones with gradual a density transition. This female subject had a scleral crescent but was not a high myope. (a) Confocal image, showing cones that guide light as bright points. (b) Scattered light image. Scale bar = 100 μm.

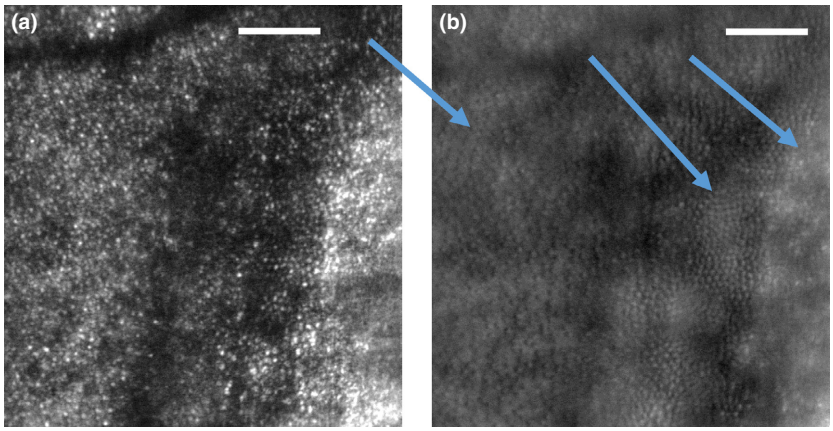


**Figure 16.** Cones at scleral crescent seen with adaptive optics scanning laser ophthalmoscope (AOSLO) imaging of cones in a female with low myopia, showing the transition from even but low density to patches of high density to scarce cones. As this is an *en face* image, this is the distribution of cones that would provide the sampling array for vision. The bright region in both images is where there is no retinal pigment epithelium (RPE) melanin. (a) Confocal image, showing cones guiding light, even over the scleral crescent. (b) Scattered light image. Blue arrows indicate low but regular density of cones, high effective density possibly on the slope of the optic nerve head, and the a lower and more irregular density of cones. Scale bar = 100 μm.

crescents were imaged with AOSLO twice each, by two operators and on successive days. For the peripapillary samples, cones were counted manually using polygonal samples that avoided unrelated fundus structure, by two graders independently. The area of each sample was computed to provide cone density in cones/mm$^2$. For the geographic atrophy data, cones were counted directly from the cone montages by another grader, using the confocal imaging method and counting software to be comparable to our published control data. A conservative approach was taken, with dark cones generally omitted. The 95% confidence limits were obtained from the entire sample of the older subjects as previously published.[47] Missing data reduced the overall degrees of freedom to 6, so that the confidence limits were computed from the average cone density $\pm$ 1.94 * S.D.

As sclera without overlying RPE is localised if high reflectivity is present (*Figures* 14–15), and is co-localised with a randomly appearing orientation of polarisation angle (*Figure* 14), both sets of subjects were imaged with our custom GDx (www.zeiss.com), using our previous methods and custom software.[51–53,58,59] For the subjects with the large peripapillary crescents, this documents the location of their scleral crescents.

For the subjects with AMD, scanning laser polarimetry documents the location of atrophy and also shows whether a macular bow-tie was present (*Figure* 19), indicating where

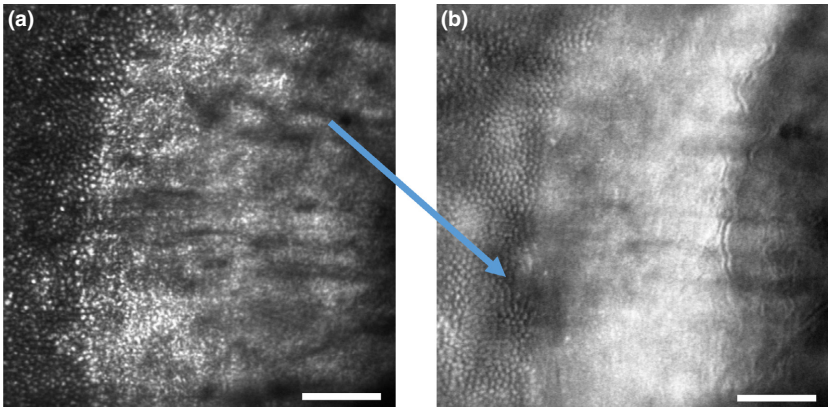


**Figure 17.** Cones at a different sampling location of the scleral crescent seen with adaptive optics scanning laser ophthalmoscope (AOSLO) imaging of cones in a female with low myopia, showing the transition from even but low density to patches of high density to scarce cones. As this is an *en face* image, this is the distribution of cones that would provide the sampling array for vision. The bright region in both images is where there is no retinal pigment epithelium (RPE) melanin. (a) Confocal image, showing cones guiding light, even over the scleral crescent. (b) Scattered light image. Blue arrow indicates a steep transition between a high density of cones and then a lower one, all over the depigmented portion of the scleral crescent. Scale bar = 100 μm.

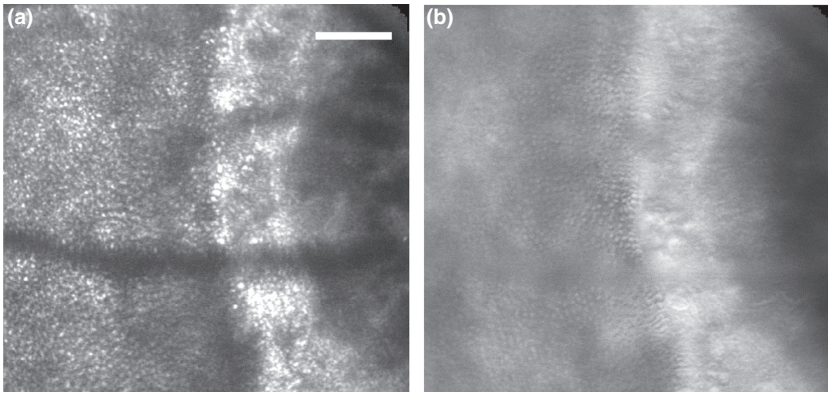


**Figure 18.** Cones at scleral crescent of the male low myope with adaptive optics scanning laser ophthalmoscope (AOSLO), showing the transition from even but low density to patches of high density to scarce cones. As this is an *en face* image, this is the distribution of cones that would provide the sampling array for vision. The bright region in both images is where there is no retinal pigment epithelium (RPE) melanin. (a) Confocal image, showing cones guiding light, even over the scleral crescent. (b) Scattered light image. Blue arrows indicate low but regular density of cones, high effective density possibly on the slope of the optic nerve head, and the a lower and more irregular density of cones. Note that the shape of cones in panel (b) is elongated, as if they are sideways, similar to the cones in the subject with the outer retinal tubulation (ORT) in Figure 10. Scale bar = 100 μm.

there was the presence of cone axons in sufficient numbers and sufficiently well-ordered to cause a macular bow tie.[51–53,55,58–60,64] The OCT data indicated considerable variation in the status of the RPE across the macula, ranging from drusen to disruption of the fundus layers to thinned or missing fundus layers (*Figure* 19). OCT was also used to determine the location of the fovea, since the foveal pit was visible in Subjects 1–3, and there was a region of thickened ONL in approximately the expected region of the fovea for all subjects (*Table* 1). Subject 2 also had primary open angle glaucoma. Three graders counted cones from the confocal images, so that the data for subjects with atrophy would match the older normative values published previously.[47] Based on our previous comparison with AOSLO cone counts and OCT layer thicknesses,[47] it is not the case that a thickened ONL consists of only cone cell bodies and could instead contain remodelled Müller cells or neurites. A sixth image grader aligned images from one modality to another, combining the AOSLO data with the scanning laser polarimetry data.

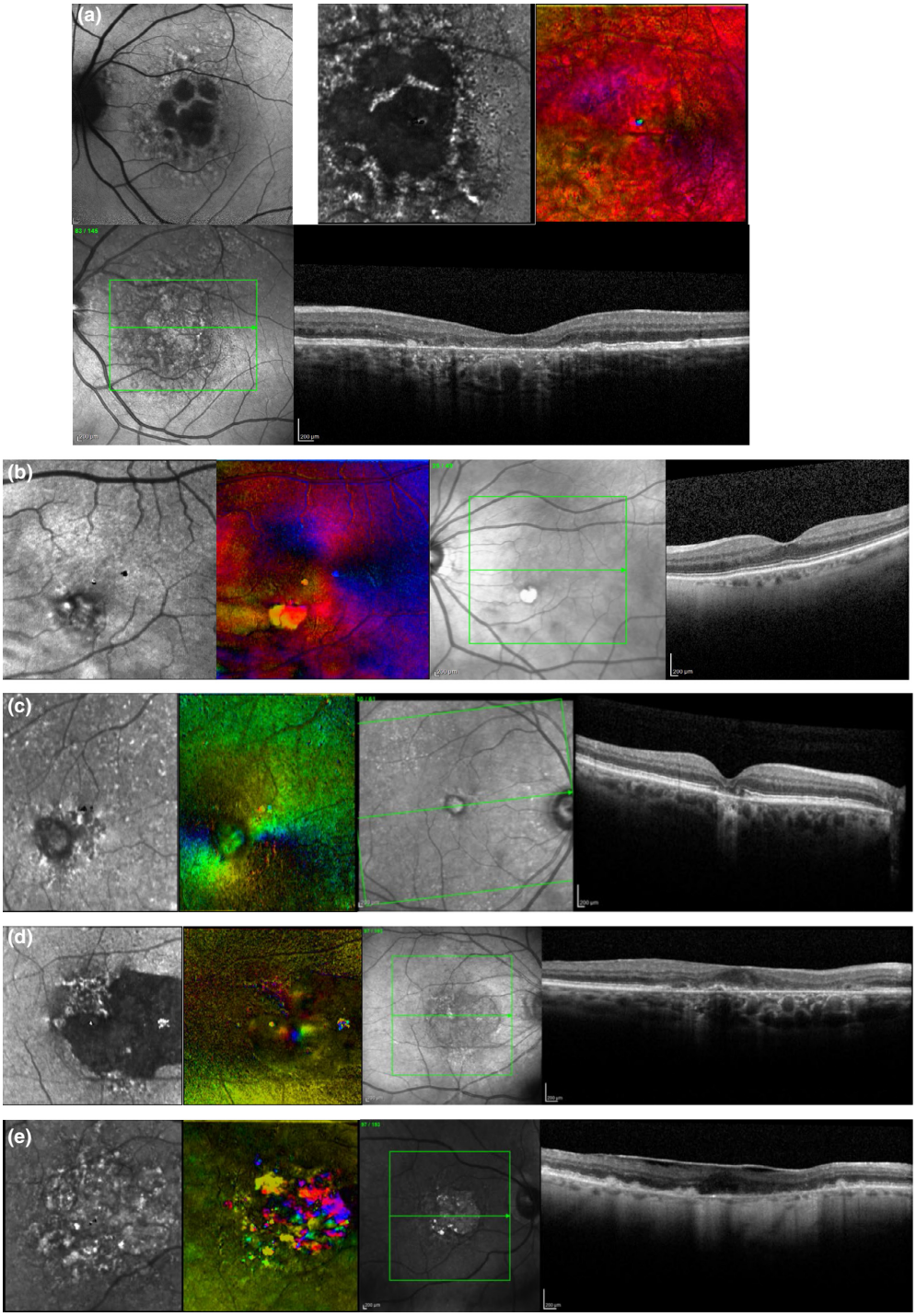


**Figure 19.** Multi-modal image to characterise the severity and location of the atrophy acquired in a similar timeframe with the adaptive optics scanning laser ophthalmoscope (AOSLO) cone counts. In order, the top or leftmost panel is the autofluorescence image at 488 nm from the Spectralis, for Subject 1 only. For all subjects, the images continue in order with the first (or next) image being two images (15 deg) from scanning laser polarimetry at 780 nm: (1) the modulation of the crossed detector, (2) the input polarisation angle that produced the maximum signal from the crossed detector, colour coded. The next image is the near-infrared reflectance (NIR) scanning laser ophthalmoscope (SLO) image from the Spectralis. The last image is the optical coherence tomography (OCT) B-scan approximately through the fovea. (a) Patient 1. (b) Patient 2, whose atrophy is most severe in the interior nasal retina. (c) Patient 3. (d) Patient 4. (e) Patient 5. Note the most severe foveal disruption in Patients 4 and 5, with Patients 1 and 3 having a foveal pit and inner retinal layers despite transmission defects.

## Results for cone imaging and quantification

The peripapillary crescent was documented as missing overlying RPE, as there was high reflectivity, high birefringence, and random appearing orientation of polarisation axis, as documented by the rapidly changing colours. Nevertheless, there were cones visualised in both confocal and multiply scattered light images that were not in direct contact with RPE (*Figures* 16–17). The cones were often sideways or enlarged. For normal retina just temporal to the optic nerve head (*Figure* 13), cone distribution appeared uniform across the entire sample. The ratio of cone density on the left side of the sample vs the right side, about 300 μm apart, was 0.83. However, for adjacent regions near the optic nerve head, the effective density of cones, i.e. cones perpendicular to the instrument regardless of the slope at the optic nerve head, had a ratio of 0.51 for the subject shown in *Figures* 16 and 17, and 1.42 for the subject in *Figure* 18.

In the patients with geographic atrophy associated with AMD, portions of the photoreceptor layer appeared distorted or missing on OCT B-scan, with transmission defects of the RPE that vary with location, as expected (*Figure* 19). The severity of the disruption to fundus layers varies across retinal location, and there are islands of better or worse RPE. The pseudocolour maps from scanning laser polarimetry visualise regions of varying and bright colour from the birefringence signal, where scleral birefringence is not blocked by RPE because the atrophy is severe (*Figure* 19). Not all subjects had the fovea as the most affected location. For all five subjects, there is a thickened region of ONL at the approximate location of a typical fovea (*Table* 1). For the three younger subjects, there is a clear-cut foveal pit and absence of an ERM sufficient to disrupt the retina layers (*Figure* 19*a–c*). For the two older subjects, there is thickened ONL on at least one B-scan near the fovea, with no foveal pit and ERM that distorts the retinal layers (*Figure* 19*d,e*).

The AOSLO images indicated that some cones were clearly present, including within the region of RPE atrophy as documented by OCT transmission defect (*Figure* 20). There was a strong birefringence signal from the region of atrophy (*Figure* 21), and despite the foveal-centred atrophy there was a macular bowtie that indicated the presence of cone axons. Cones could be counted in many regions, but not all. Cones were not found in the normal distribution, or even the typical slowly varying distribution (*Figures* 21–22). Cones could have regular arrays, seen in both confocal and multiply scattered light imaging even over patches of transmission defects and scattered light (*Figure* 22). The cones in the fovea region were below the normal limits for older subjects, if countable. However, for subjects 1, 2, and 4, the cone density counts were higher than the normal limits at some locations eccentric to the fovea, e.g. about 4–5 deg (*Figure* 23). In retinal regions away from the most severe atrophy, cone densities were typically at least as great as the normative values. Cones outside of the most severe atrophy could have a regular array and high density (*Figure* 23*f*).

**Table 1.** Characteristics of patients with geographic atrophy

| Subject | Age in years | VA in test eye | ERM?† | Bowtie? | ONL thicker? |
|---|---|---|---|---|---|
| 1 | 66 | 20/30+1 | N | Y | Y |
| 2 | 73 | 20/30 | N | Y | Y |
| 3 | 73 | 20/30−2 | N | Y | Y |
| 4 | 82 | 20/40−1 | Y | N | Y |
| 5 | 82 | 20/50 | Y | N | Y |

†Epiretinal membrane.

## Methods for measuring changes in cone length with ageing

The neural economy hypothesis predicts that older subjects would have shorter photoreceptors. OCT data from the eigth younger 24–32 years, mean 27.2) and eight older subjects aged 51–65 years, mean 56.2) tested previously[47,83] for cone density and relative ONL and other layer thicknesses were resegmented with custom software (MATLAB, www.mathworks.com). All subjects received a complete eye examination, including a subjective refraction and fundus examination. All subjects had best corrected visual acuity of 6/6 (20/20) or better and were phakic. Exclusion criteria were any evidence of retinal pathology or systemic diseases. Further, we reduced the variability in cone density and ONL or HFL thickness due to eye shape or eye elongation by limiting refractive error. Spherical equivalent refractive errors ranged from +1.00 to −3.75 dioptres (D, younger subjects +1.00 to −3.00 D, mean ± 0.28 D; older subjects +2.50 to −3.75 D, mean ± 1.03 D) with astigmatism less than −1.00 D when referenced to the spectacle plane, and axial lengths greater than 26.5 mm were excluded. The length of the inner segments of photoreceptors and the outer segments of photoreceptors were quantified and compared. For the outer segments, the measurement extended in the B-scan from the outer part of the photoreceptor/RPE interdigitation zone to the outermost boundary of the ellipsoid zone. For the inner segments, the measurement extended from the outermost boundary of the ellipsoid zone to the external limiting membrane (ELM). Measurements were made at 15 locations (0 ± 4.9 deg).

## Results for measuring changes in cone length with ageing

The ratio of photoreceptor length for older:younger subject groups was significantly less than 1 if averaged across all 15

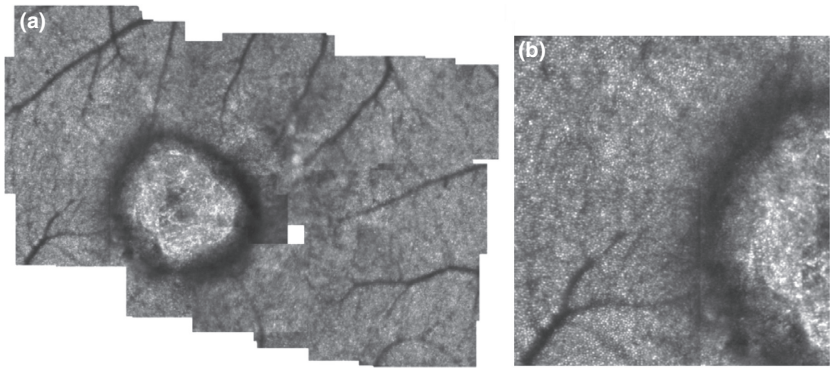


**Figure 20.** Confocal images showing cones in atrophy in Patient 3 from Figure 19 and Table 1. (a) The cone montage method removes uncertainty about retinal location. (b) Enlargement of a portion of the atrophic retina and more normal retina, showing that cones that are less dense within the atrophy, but guiding light and readily counted despite retinal pigment epithelium (RPE) transmission defects on optical coherence tomography (OCT).

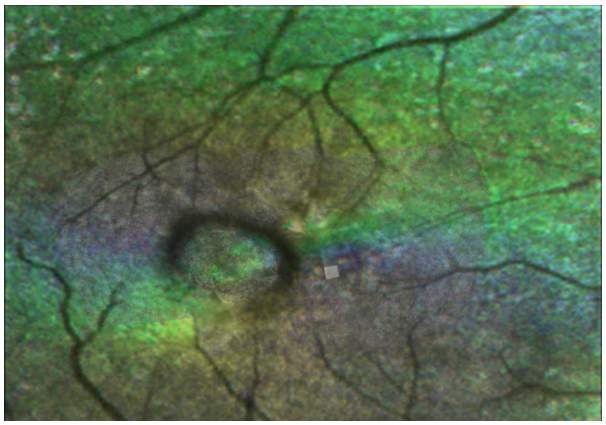

**Figure 21.** Confocal images showing cones in atrophy in Patient 3, from Figure 19 and Table 1, combined with the results from scanning laser polarimetry. The presence of the macular bowtie indicates that Henle fibres are present and measureable. Despite the significant retinal pigment epithelium (RPE) transmission defect on the optical coherence tomography (OCT) B-scan, the cones can be counted and their axons are present.

locations (±4.9 deg from the fovea) for the inner, outer, and total (inner + outer) length measurements ($p$ = 0.0015, 0.037, and 0.0015, respectively) (*Figure* 24).

## Discussion

These results document that cones survive in some eyes that have missing or diseased RPE, and can be found in regular arrays. Sometimes cone density outside the fovea is comparable or greater than the normative values, but the rapid change in density over space outside the fovea is abnormal. In some eyes with geographic atrophy, there appears to be a survival of inner retinal layers that could be capable of supporting cone pathway vision. Ageing changes do exist, with fewer cones or shorter cones for older subjects than younger ones. However, in our small sample, the regular arrays of cones found despite diseased RPE indicate the potential for vision. This is consistent with data we have collected over many years using multiple measurement modalities.

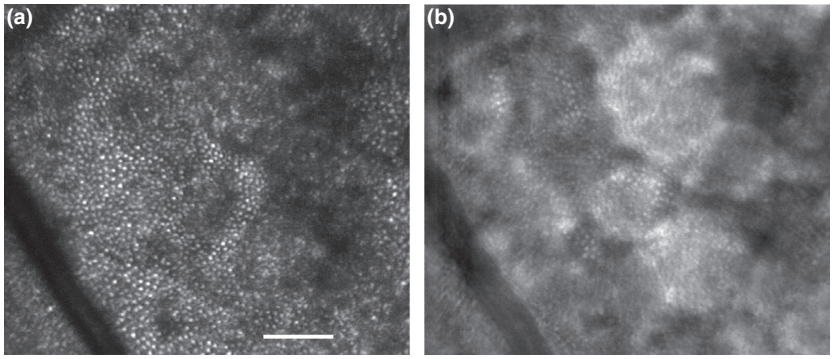


**Figure 22.** Adaptive optics scanning laser ophthalmoscope (AOSLO) images showing cones in atrophy in Patient 1, comparing the cones with confocal imaging and cones seen in scattered light. (a) There are several patches of regular arrays of cones, which guide light in confocal imaging. (b) There are several patches of regular arrays of cones, seen over whitish regions indicating scattered light from lack of retinal pigment epithelium (RPE) absorption. The cones are seen as small bumps. The scale bar is 100 μm.

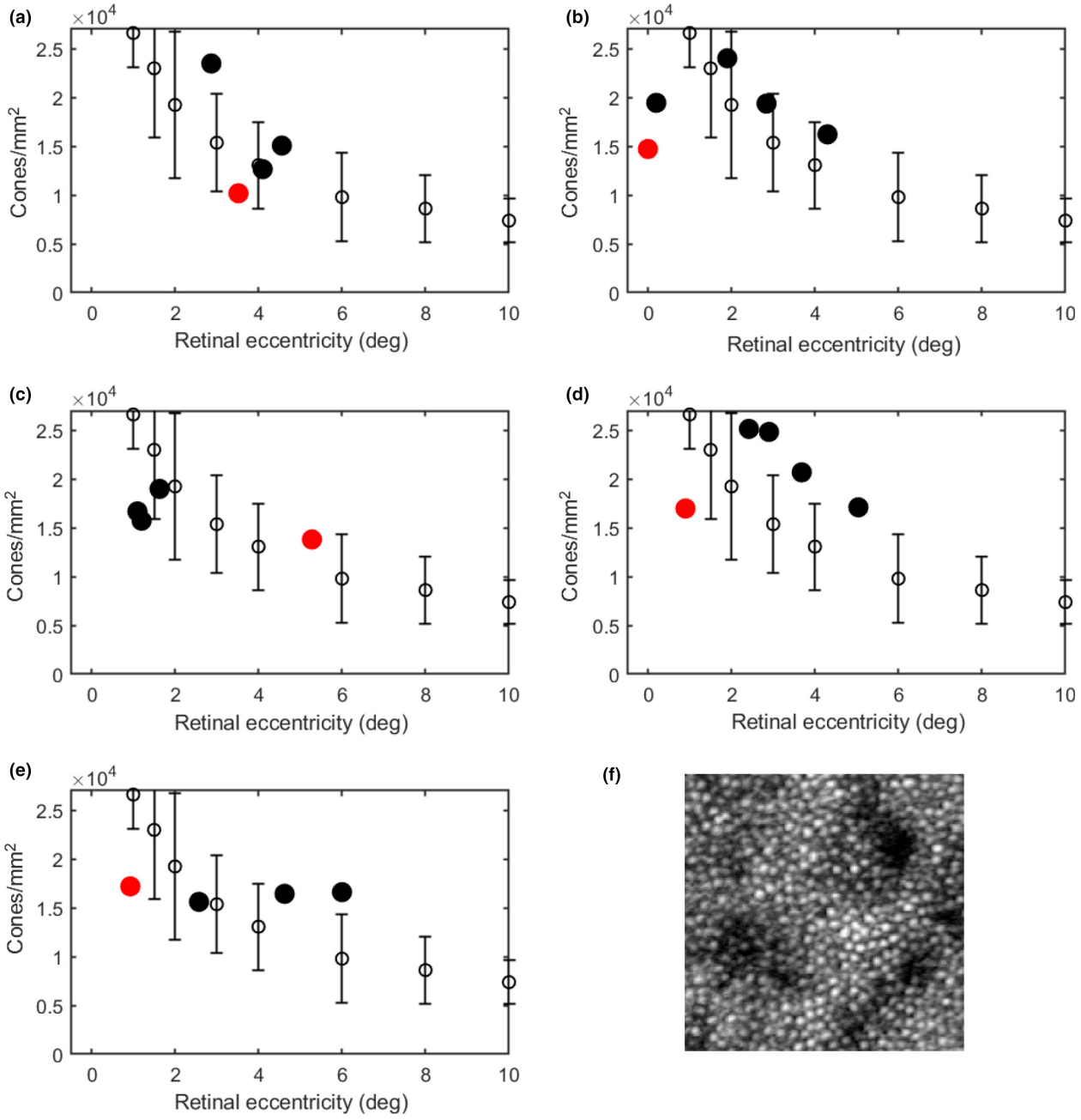


**Figure 23.** Cones density for subject 1 (a), 2 (b), (c), 4 (d), and 5 (e) The cones in the adaptive optics scanning laser ophthalmoloscope (AOSLO) images, measured in cones/mm$^2$, were significantly less dense when located in atrophy in or near the fovea (red circles) compared with those of the older controls (open symbols with error bars). For more eccentric cones, whether in only partial atrophy or within a more normal appearing microenvironment, cone densities were routinely at least within normal limits (filled black symbols). The cones in subjects with atrophy were significantly greater than for controls for some retinal locations, e.g. Subjects 1, 2, and 4. (f) AOSLO image of cones for subject 1, showing the regular and unusually dense cone array at 5.2 deg temporal, despite near-by atrophy. This image subtends 200 × 200 μm on the retina.

The potential for vision in a patient with AMD, who has had RPE changes for decades, may not match that of a young, healthy individual for several reasons. First, many patients even in early AMD have lower photopigment optical density in their individual cones than do young, normal subjects or older subjects.[61,67,68,92] The decreased photopigment optical density may be due to optical pathlength changes for cones that are distorted over drusen and hyperpigmentation. Similarly, decreased waveguiding is expected in cones with fewer segments.[92] In addition to decreased

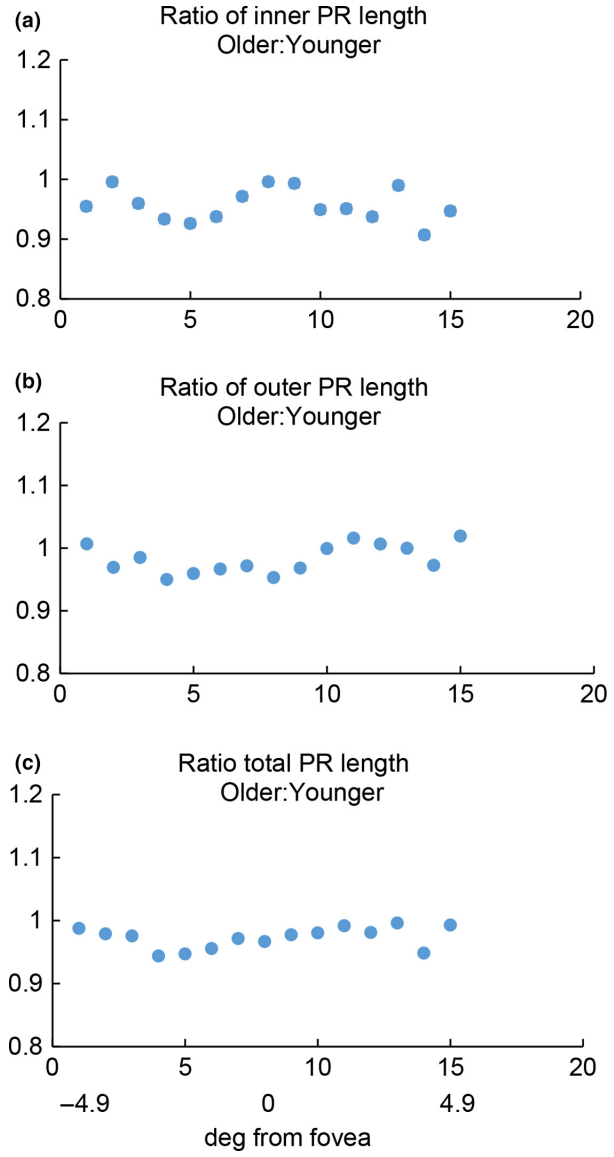


**Figure 24.** The ratio of the length measurements plotted for retinal location in deg from the fovea, sampled at each 0.5 deg around the fovea, which is position 8. The average ratio at each location is typically less than one for older vs younger subjects for photoreptor (PR) (a) inner segments, (b) outer segments, and (c) the total as measured by optical coherence tomography (OCT) B-scan for younger vs older subjects. Error bars are ± 1 normalised Standard Error of the Mean.

sensitivity and a spectral shift due to decreased self-screening by photopigment, a decrease in waveguiding also can lead to poor spatial separation of light captured by adjacent cones. Thus, reduced waveguiding can lead to decreases in spatial resolution and contrast on the retina, and changes in colour vision.

The interaction of rod and cone pathways occurs at virtually every stage in the retina,[93] making difficult the prediction of visual function following the loss of photoreceptors. The imaging of cones nearer vs farther from the fovea (*Figure* 9) clearly indicates the potential for much more interaction among rods and cones outside the fovea. There is still the potential retention of cone-cone interactions even outside the fovea, by means of lateral processes such as teleodendrites. By studying mesopic vision to include both rod and cone responses,[94] it becomes clear that rods play a role in colour vision, and not just light adaptation. The differing characteristics of rods vs cones for light level, wavelength, retinal eccentricity, and temporal and spatial aspects of vision result in functional differences between controls and patients with AMD for scotopic, mesopic, and photopic mechanisms, along with adaptation, colour contrast, acuity, etc.[95,96]

In addition to retinal remodelling that occurs with loss of neurons,[84] there is the potential for binocular summation or inhibition, with differences due to binocular disparity, spatial frequency, and eccentricity.[97] In patients with geographic atrophy and AMD, potential vision is not accurately assessed by limiting measurements only to initial ones. Experience of these patients over 1–2 years has shown that visual acuity measurements improve without anatomical improvement.[98] In this longitudinal study of better vs worse-seeing eyes, 5 of 48 worse-seeing eyes with baseline visual acuity improved 10 or more letters by the 2 years follow-up. One explanation is that the subject learned to use a better preferred retinal locus for the reading of letters. Alternatively, or in addition, the subject may have some visual input from the region of the scotoma and has learned not to suppress the previously poorer input from the first eye that lost substantial visual acuity when the second eye develops reduced visual acuity.[98,99] Similarly, despite large central scotomata, 18 of 20 subjects with AMD could be trained with SLO presentation of text to use a better preferred retinal locus, thereby increasing their reading speeds both significantly and to a useful level.[100] This is consistent with the findings noted above with simultaneous retinal imaging, i.e. that subjects sometimes retained sensitivity over or quite near severe fundus lesions[73] and that subjects used clusters of fixation points amid atrophy.[35]

Potential vision from surviving cones may not always be a positive outcome for a patient, as this imperfect visual input may be a negative factor in patients who are older and have AMD. Large numbers of patients experience visual hallucinations, known as Charles Bonnet syndrome.[101,102]

To understand the impact of potentially delaying an extreme loss of cones, we investigated the prevalence and causes of moderate to severe sight threatening visual impairment in 191 000 000 patients globally. We summarised two literature sources that are inexplicably isolated from each other: vision screening, particularly for diabetic

retinopathy, and population-based epidemiological studies.[103] To foster communication between these segregated fields and call attention to the growing need for eyecare worldwide, we selected a high proportion of references from open access sources. Further, to show the power of modern imaging, we provided examples from the advanced imaging technologies described in this paper, which elucidate the underlying biology of retinal diseases in living humans. We found that AMD remains the chief cause of untreatable visual impairment, except for degenerative myopia in some Asian populations including those living in Europe. Again, the degeneration of the RPE is a potential threat to vision. Advanced imaging techniques have allowed the documentation of changes to the retina, RPE, and choroid far beyond ophthalmic examination or colour fundus photography, due to the limitations of imaging with visible wavelength light. We document the harsh environment of cones, with NIR imaging[17,41,46] and multi-mode imaging[17,41,45,46,103]: drusen, RPE damage, layer distortions, and fluid within retinal layers.

Diabetic retinopathy and diabetic macular oedema are also chief causes of macular impairment.[103] Although glaucoma has a high prevalence, we found that screening studies often do not address peripheral vision loss. Most studies included adults, but not children.

Many studies indicated that the likelihood of sight threatening visual impairment is increasing with increasing age. This body of literature points to the unmet need of understanding how vision is impaired throughout disease progression, and what might slow, halt, reverse, or rehabilitate vision loss. Further, as the chief causes of macular impairment destroy vision over decades, more emphasis is needed on preserving or restoring vision long after the initial events in the disease pathways. Preserving cones, which have remarkable survival powers, could help patients retain vision in a wide variety of diseases.

## Acknowledgements

This work was supported by NIH NEI EY07624, EY04395, EY024315, EY024186, EY01867, and EY030829.

## Disclosure

Dr Elsner is a principal investor in Aeon Imaging, LLC, which builds retinal imaging and display devices, some of which are among the many technologies described herein. Mr. Muller is also an investor, Dr Gast and Mr Papay are employees, and Dr Burns is the spouse of Dr Elsner. The authors report no conflicts of interest and have no proprietary interest in any of the materials mentioned in this article.

## References

1. Strauss O. The retinal pigment epithelium in visual function. *Physiol Rev* 2005; 85: 845–881.
2. Bearelly S, Chau FY, Koreishi A, Stinnett SS, Izatt JA & Toth CA. Spectral domain optical coherence tomography imaging of geographic atrophy margins. *Ophthalmology* 2009; 116: 1762–1769.
3. Sarks JP, Sarks SH & Killingsworth MC. Evolution of geographic atrophy of the retinal pigment epithelium. *Eye (Lond)* 1988; 2: 552–577.
4. Jonas JB, Ohno-Matsui K, Spaide RF, Holbach L & Panda-Jonas S. Macular Bruch's membrane defects and axial length: association with gamma zone and delta zone in peripapillary region. *Invest Ophthalmol Vis Sci* 2013; 54: 1295–1302.
5. Dichtl A, Jonas JB & Naumann GO. Histomorphometry of the optic disc in highly myopic eyes with absolute secondary angle closure glaucoma. *Br J Ophthalmol* 1998; 82: 286–289.
6. Bejarano-Escobar R, Sánchez-Calderón H, Otero-Arenas J, Martín-Partido G & Francisco-Morcillo J. Müller glia and phagocytosis of cell debris in retinal tissue. *J Anat* 2017; 231: 471–483.
7. Mata NL, Radu RA, Clemmons RC & Travis GH. Isomerization and oxidation of vitamin a in cone- dominant retinas: a novel pathway for visual-pigment regeneration in daylight. *Neuron* 2002; 36: 69–80.
8. Mata NL, Ruiz A, Radu RA, Bui TV & Travis GH. Chicken retinas contain a retinoid isomerase activity that catalyzes the direct conversion of all-trans-retinol to 11-cis-retinol. *Biochemistry* 2005; 44: 11715–11721.
9. Sakami S, Imanishi Y & Palczewski K. Müller glia phagocytose dead photoreceptor cells in a mouse model of retinal degenerative disease. *FASEB J* 2019; 33: 3680–3692.
10. Zhao L, Zabel MK, Wang X *et al.* Microglial phagocytosis of living photoreceptors contributes to inherited retinal degeneration. *EMBO Mol Med* 2015; 7: 1179–1197.
11. Schuman SG, Koreishi AF, Farsiu S, Jung SH, Izatt JA & Toth CA. Photoreceptor layer thinning over drusen in eyes with age-related macular degeneration imaged in vivo with spectral-domain optical coherence tomography. *Ophthalmology* 2009; 116: 488–496.
12. Punzo C, Xiong W & Cepko CL. Loss of daylight vision in retinal degeneration: are oxidative stress and metabolic dysregulation to blame? *J Biol Chem* 2012; 287: 1642–1648
13. Forooghian F, Stetson PF, Meyer SA *et al.* Relationship between photoreceptor outer segment length and visual acuity in diabetic macular edema. *Retina* 2010; 30: 63–70.
14. Elsner AE, Burns SA & Weiter JJ. Retinal densitometry in retinal tears and detachments. *Clinical Vis Sci* 1992; 7: 489–500.
15. Hendrickson A, Possin D, Vajzovic L & Toth CA. Histologic development of the human fovea from midgestation to maturity. *Am J Ophthalmol* 2012; 154: 767–778.

16. Elsner AE, Burns SA, Delori FC & Webb RH. Quantitative reflectometry with the SLO. In: *Laser Scanning Ophthalmoscopy and Tomography*. Quintessenz-Verlag: Munich, 1990, (Nasemann JE & Burk ROW, editors), pp. 109–121.
17. Elsner AE, Burns SA, Weiter JJ & Delori FC. Infrared imaging of sub-retinal structures in the human ocular fundus. *Vision Res* 1996; 36: 191–205.
18. Remky A, Elsner AE, Morandi AJ, Beausencourt E & Trempe CL. Blue-on-yellow perimetry with a scanning laser ophthalmoscope: small alterations in the central macula with aging. *J Opt Soc Am A Opt Image Sci Vis* 2001; 18: 1425–1436.
19. Elsner AE, Burns SA, Hughes GW & Webb RH. Reflectometry with a scanning laser ophthalmoscope. *Appl Opt* 1992; 31: 3697–3710.
20. Miura M, Elsner AE, Osako M *et al*. Spectral imaging of the area of internal limiting membrane peeling. *Retina* 2005; 25: 468–472.
21. Elsner AE, Burns SA & Webb RH. Mapping cone photopigment density in humans. *J Opt Soc Am A* 1993; 10: 52–58.
22. Elsner AE, Jalkh AH & Weiter JJ. New devices in retinal imaging and functional evaluation. In: *Practical Atlas of Retinal Disease and Therapy*. New York, NY: Raven, 1993, (Freeman W, editor), pp. 19–35.
23. Marcos S, Tornow R-P, Elsner AE & Navarro R. Foveal cone spacing and cone photopigment density difference: objective measurements in the same subjects. *Vision Res* 1997; 37: 1909–1915.
24. Elsner AE, Bartsch D-U, Weiter JJ & Hartnett ME. New devices in retinal imaging and functional evaluation. In: *Practical Atlas of Retinal Disease and Therapy*, 2nd edn. New York, NY: Lippincott-Raven, 1998, (Freeman W, editor), pp. 19–55.
25. Elsner AE. Fundamental properties of the retina. In: *Adaptive Optics for Vision Science: Principles, Practices, Design, and Applications*. John Wiley & Sons, Inc.: Hoboken, NJ, 2006, (Porter J, Queener H, Lin J, Thorn K & Awwal A, editors), pp. 205–234.
26. Huang D, Swanson EA, Lin CP *et al*. Optical coherence tomography. *Science* 1991; 254: 1178–1181.
27. Elsner AE & Muller MS. Laser applications and system considerations in ocular imaging. *Laser Photon Rev* 2008; 2: 350–376.
28. Kashani AH, Chen CL, Gahm JK *et al*. Optical coherence tomography angiography: a comprehensive review of current methods and clinical applications. *Prog Retin Eye Res* 2017; 60: 66–100.
29. Nesper PL, Soetikno BT, Zhang HF & Fawzi AA. OCT angiography and visible-light OCT in diabetic retinopathy. *Vision Res* 2017; 139: 191–203.
30. Spaide RF, Fujimoto JG, Waheed NK, Sadda SR & Staurenghi G. Optical coherence tomography angiography. *Prog Retin Eye Res* 2018; 64: 1–55.
31. Arthur E, Elsner AE, Sapoznik KA, Papay JA, Muller MS & Burns SA. Distances from capillaries to arterioles or venules measured using OCTA and AOSLO. *Invest Ophthalmol Vis Sci* 2019; 60: 1833–1844.
32. Staurenghi G, Sadda S, Chakravarthy U & Spaide RF. International Nomenclature for Optical Coherence Tomography (IN•OCT) Panel. Proposed lexicon for anatomic landmarks in normal posterior segment spectral-domain optical coherence tomography: the IN•OCT consensus. *Ophthalmology* 2014; 121: 1572–1578.
33. Burns SA, Elsner AE, Sapoznik KA, Warner RL & Gast TJ. Adaptive optics imaging of the human retina. *Prog Retin Eye Res* 2019; 68: 1–30.
34. Ferguson R, Hammer D, Elsner A, Webb R, Burns S & Weiter J. Wide-field retinal hemodynamic imaging with the tracking scanning laser ophthalmoscope. *Opt Express* 2004; 12: 5198–5208.
35. Elsner AE, Petrig BL, Papay JA, Kollbaum EJ, Clark CA & Muller MS. Fixation stability and scotoma mapping for patients with low vision. *Optom Vis Sci* 2013; 90: 164–173.
36. Muller MS, Green JJ, Baskaran K *et al*. Non-mydriatic confocal retinal imaging using a digital light projector. *Proc SPIE Int Soc Opt Eng* 2015; 9376: 93760E.
37. Muller MS & Elsner AE. Confocal retinal imaging using a digital light projector with a near infrared VCSEL source. *Proc SPIE Int Soc Opt Eng* 2018; 10546: 105460G.
38. Elsner AE, Miura M, Burns SA *et al*. Multiply scattered light tomography and confocal imaging: detecting neovascularization in age-related macular degeneration. *Opt Express* 2000; 7: 95–106.
39. Elsner AE, Zhou Q, Beck F *et al*. Detecting AMD with multiply scattered light tomography. *Int Ophthalmol* 2001; 23: 245–250.
40. Anderson DH, Radeke MJ, Gallo NB *et al*. The pivotal role of the complement system in aging and age-related macular degeneration: hypothesis re-visited. *Prog Retin Eye Res* 2010; 29: 95–112.
41. Hartnett EM & Elsner AE. Characteristics of exudative age-related macular degeneration determined in vivo with confocal direct and indirect infrared imaging. *Ophthalmology* 1996; 103: 58–71.
42. Miura M, Elsner AE, Beausencourt E *et al*. Grading of infrared confocal scanning laser tomography and video displays of digitized color slides in exudative age-related macular degeneration. *Retina* 2002; 22: 300–308.
43. Hartnett ME, Weiter JJ, Staurenghi G & Elsner AE. Deep retinal vascular anomalous complexes in advanced age-related macular degeneration. *Ophthalmology* 1996; 103: 2042–2053.
44. Folgar FA, Chow JH, Farsiu S *et al*. Spatial correlation between hyperpigmentary changes on color fundus photography and hyperreflective foci on SDOCT in intermediate AMD. *Invest Ophthalmol Vis Sci* 2012; 53: 4626–4633.
45. Miura M, Makita S, Sugiyama S *et al*. Evaluation of intraretinal migration of retinal pigment epithelial cells in age-related macular degeneration using polarimetric imaging. *Sci Rep* 2017; 7: 3150.

46. Elsner AE, Moraes L, Beausencourt E *et al*. Scanning laser reflectometry of retinal and subretinal tissues. *Opt Express* 2000; 6: 243–250.
47. Chui TY, Song H, Clark CA, Papay JA, Burns SA & Elsner AE. Cone photoreceptor packing density and the outer nuclear layer thickness in healthy subjects. *Invest Ophthalmol Vis Sci* 2012; 53: 3545–3553.
48. Zweifel SA, Engelbert M, Laud K, Margolis R, Spaide RF & Freund KB. Outer retinal tubulation: a novel optical coherence tomography finding. *Arch Ophthalmol* 2009; 127: 1596–1602.
49. King BJ, Sapoznik KA, Elsner AE *et al*. OCT and adaptive optics imaging of outer retinal tubulation. *Vis Sci* 2017; 94: 411–422.
50. Arthur E, Papay JA, Haggerty BP, Clark CA & Elsner AE. Subtle changes in diabetic retinas localised in 3D using OCT. *Ophthalmic Physiol Opt* 2018; 38: 477–491.
51. Elsner AE, Miura M, Stewart JB, Kairala MB & Burns SA. Novel algorithms for polarization imaging resulting in improved quantification of retinal blood vessels. *Stud Health Technol Inform* 2003; 94: 59–61.
52. Elsner AE, Weber A, Cheney MC, VanNasdale DA & Miura M. Imaging polarimetry in patients with neovascular age-related macular degeneration. *J Opt Soc Am A Opt Image Sci Vis* 2007; 24: 1468–1480.
53. Elsner AE, Weber A, Cheney MC & VanNasdale DA. Spatial distribution of macular birefringence associated with the Henle fibers. *Vision Res* 2008; 48: 2578–2585.
54. Weber A, Cheney MC, Smithwick QYJ & Elsner AE. Polarimetric imaging and blood vessel quantification. *Opt Express* 2004; 12: 5178–5190.
55. Weber A, Elsner AE, Mirua M, Kompa S & Cheney MC. Relationship between foveal birefringence and visual acuity in neovascular age-related macular degeneration. *Eye (Lond)* 2007; 21: 3533–3561.
56. Miura M, Elsner AE, Cheney MC, Usui M & Iwasaki T. Imaging polarimetry and retinal blood vessel quantification at the epiretinal membrane. *J Optical Soc Am A Opt Image Sci Vis* 2007; 24: 1431–1437.
57. Miura M, Yamanari M, Iwasaki T *et al*. Imaging polarimetry in age-related macular degeneration. *Invest Ophthalmol Vis Sci* 2008; 49: 2661–2667.
58. VanNasdale DA, Elsner AE, Weber A, Miura M & Haggerty BP. Determination of foveal location using scanning laser polarimetry. *J Vis* 2009; 9: 1–17.
59. VanNasdale DA, Elsner AE, Kohne KD *et al*. Foveal localization in non-exudative AMD using scanning laser polarimetry. *Optom Vis Sci* 2012; 89: 667–677.
60. VanNasdale DA, Elsner AE, Hobbs T & Burns SA. Foveal phase retardation changes associated with normal aging. *Vision Res* 2011; 51: 2263–2272.
61. Elsner AE, Burns SA, Beausencourt E & Weiter JJ. Foveal cone photopigment distribution: small alterations associated with macular pigment distribution. *Invest Ophthalmol Vis Sci* 1998; 39: 2394–2404.
62. Burns SA, Elsner AE, Mellem-Kairala MB & Simmons RB. Improved contrast of subretinal structures using polarization analysis. *Invest Ophthalmol Vis Sci* 2003; 44: 4061–4068.
63. Mellem-Kairala MB, Elsner AE, Weber A, Simmons RB & Burns SA. Improved contrast of peripapillary hyperpigmentation using polarization analysis. *Invest Ophthalmol Vis Sci* 2005; 46: 1099–1106.
64. VanNasdale DA, Elsner AE, Malinovsky VE *et al*. Polarization variability in age-related macular degeneration. *Optom Vis Sci* 2018; 95: 277–291.
65. Papay JA & Elsner AE. Near-infrared polarimetric imaging and changes associated with normative aging. *J Opt Soc Am A Opt Image Sci Vis* 2018; 35: 1487–1495.
66. Burns SA, Elsner AE, Lobes LA Jr & Doft BH. A psychophysical technique for measuring cone photopigment bleaching. *Invest Ophthalmol Vis Sci* 1987; 28: 711–717.
67. Elsner AE, Berk L, Burns SA & Rosenberg PR. Aging and human cone photopigments. *J Opt Soc Am A* 1988; 5: 2106–2112.
68. Elsner AE, Burns SA & Weiter JJ. Cone photopigment in older subjects: decreased optical density in early age-related macular degeneration. *J Opt Soc Am A* 2002; 19: 215–222.
69. Timberlake GT, Mainster MA, Peli E, Augliere RA, Essock EA & Arend LE. Reading with a macular scotoma. I. Retinal location of scotoma and fixation area. *Invest Ophthalmol Vis Sci* 1986; 27: 1137–1147.
70. Remky A, Beausencourt E & Elsner AE. Angioscotometry with the scanning laser ophthalmoscope. Comparison of the effect of different wavelengths. *Invest Ophthalmol Vis Sci* 1996; 37: 2350–2355.
71. Remky A & Elsner AE. Blue on yellow perimetry with scanning laser ophthalmoscopy in patients with age related macular disease. *Br J Ophthalmol* 2005; 89: 464–469.
72. Chen J-F, Elsner AE, Burns SA *et al*. The effect of eye shape on retinal responses. *Clin Vis Sci* 1992; 7: 521–530.
73. Moraes L, Elsner AE, Kunze C *et al*. Evaluation of macular perimetry in patients with age-related macular degeneration using the scanning laser ophthalmoscope. *Arq Bras Oftalmol* 2007; 70: 844–850.
74. Arend O, Wolf S, Jung F *et al*. Retinal microcirculation in patients with diabetes mellitus: dynamic and morphological analysis of perifoveal capillary network. *Br J Ophthalmol* 1991; 75: 514–518.
75. Bradley A, Zhang H, Applegate RA,Thibos LN & Elsner AE. Entoptic image quality of the retinal vasculature. *Vision Res* 1998; 8: 2685–2696.
76. Wolf S, Remky A, Elsner AE, Arend O & Reim M. Indocyanine green video angiography in patients with retinal pigment epithelial detachments. *Ger J Ophthalmol* 1994; 3: 224–227.
77. Grunwald JE, Hariprasad SM, DuPont J *et al*. Foveolar choroidal blood flow in age-related macular degeneration. *Invest Ophthalmol Vis Sci* 1998; 39: 385–390.

78. Burns SA, Wu S, Delori FC & Elsner AE. Direct measurement of human cone photoreceptor alignment. *J Opt Soc Am A* 1995; 12: 2329–2338.
79. Burns SA, Marcos S, Elsner AE & Barra S. Contrast improvement for confocal retinal imaging using phase correcting plates. *Opt Lett* 2002; 27: 400–402.
80. Burns SA, Elsner AE, Chui TY *et al*. In vivo adaptive optics microvascular imaging in diabetic patients without clinically severe diabetic retinopathy. *Biomed Opt Express* 2014; 5: 961–974.
81. Elsner AE, Chui TYP, Feng L, Song HX, Papay JA & Burns SA. Distribution differences of macular cones measured by AOSLO: variation in slope from fovea to periphery more pronounced than differences in total cones. *Vision Res* 2017; 132: 62–68.
82. Chui TYP, Song H & Burns SA. Individual variations in human cone photoreceptor packing density: variations with refractive error. *Invest Ophthalmol Vis Sci* 2008; 49: 4679–4687.
83. Song H, Chui TY, Zhong Z, Elsner AE & Burns SA. Variation of cone photoreceptor packing density with retinal eccentricity and age. *Invest Ophthalmol Vis Sci* 2011; 52: 7376–7384.
84. Jones BW, Pfeiffer RL, Ferrell WD, Watt CB, Tucker J & Marc RE. Retinal remodeling and metabolic alterations in human AMD. *Front Cell Neurosci* 2016; 10: 103.
85. Cideciyan AV, Swider M, Aleman TS *et al*. ABCA4-associated retinal degenerations spare structure and function of the human parapapillary retina. *Invest Ophthalmol Vis Sci* 2005; 46: 4739–4746.
86. Scoles D, Sulai YN, Langlo CS *et al*. In vivo imaging of human cone photoreceptor inner segments. *Invest Ophthalmol Vis Sci* 2014; 55: 4244–4351.
87. de Castro A, Sawides LQ & X & Burns, SA. . Adaptive optics retinal imaging with automatic detection of the pupil and its boundary in real time using Shack Hartmann images. *Appl Opt* 2017; 56: 6748–6754.
88. Grunwald JE, Daniel E, Huang J *et al*. Risk of geographic atrophy in the comparison of age-related macular degeneration treatments trials. *Ophthalmology* 2014; 121: 150–161.
89. Sawides L, Sapoznik KA, de Castro A *et al*. Alterations to the foveal cone mosaic of diabetic patients. *Invest Ophthalmol Vis Sci* 2017; 58: 3395–3403.
90. Gao SS, Jia Y, Zhang N *et al*. Optical coherence tomography angiography. *Invest Ophthalmol Vis Sci* 2016; 57: 4485–4492.
91. Waheed NK, Moult EM, Fujimoto JG & Rosenfeld PJ. Optical coherence tomography angiography of dry age-related macular degeneration. *Dev Ophthalmol* 2016; 56: 91–100.
92. Smith VC, Pokorny J & Diddie KR. Color matching and the Stiles-Crawford effect in observers with early age-related macular changes. *J Opt Soc Am A* 1988; 5: 2113–2121.
93. Fain G & Sampath AP. Rod and cone interactions in the retina [version 1; peer review: 4 approved]. *F1000Res* 2018; 7: 657.
94. Stockman A & Sharpe LT. Into the twilight zone: the complexities of mesopic vision and luminous efficiency. *Ophthalmic Physiol Opt* 2006; 26: 225–239.
95. Cocce KJ, Stinnett SS, Luhmann UFO *et al*. Visual function metrics in early and intermediate dry age-related macular degeneration for use as clinical trial endpoints. *Am J Ophthalmol* 2018; 189: 127–138.
96. Tahir HJ, Rodrigo-Diaz E, Parry NRA *et al*. Slowed dark adaptation in early AMD: dual stimulus reveals scotopic and photopic abnormalities. *Invest Ophthalmol Vis Sci* 2018; 59: AMD202–AMD210.
97. Alberti CF & Bex PJ. Binocular contrast summation and inhibition depends on spatial frequency, eccentricity and binocular disparity. *Ophthalmic Physiol Opt* 2018; 38: 525–537.
98. Sunness JS. Spontaneous improvement in visual acuity in age-related geographic atrophy of the macula. *JAMA Ophthalmol* 2014; 132: 356–357.
99. Pfau M, von der Emde L, Dysli C *et al*. Light sensitivity within areas of geographic atrophy secondary to age-related macular degeneration. *Invest Ophthalmol Vis Sci* 2019; 60: 3992–4001.
100. Nilsson UL, Frennesson C & Nilsson SE. Patients with AMD and a large absolute central scotoma can be trained successfully to use eccentric viewing, as demonstrated in a scanning laser ophthalmoscope. *Vision Res* 2003; 43: 1777–1787.
101. Carpenter K, Jolly JK & Bridge H. The elephant in the room: understanding the pathogenesis of Charles Bonnet syndrome. *Ophthalmic Physiol Opt* 2019; 39: 414–421.
102. Niazi S, Krogh Nielsen M, Singh A, Sørensen TL & Subhi Y. Prevalence of Charles Bonnet syndrome in patients with age-related macular degeneration: systematic review and meta-analysis. *Acta Ophthalmol* 2019. [Epub ahead of print]. https://doi.org/10.1111/aos.14287
103. Elsner AE & King BJ. Screening for macular disorders: the optometrist's perspective. *Clinical Optometry* 2015; 7: 15–38.

**Ann E Elsner** is a Professor at the Indiana University School of Optometry in Bloomington, Indiana, USA. She received her B.A. degree from Indiana University, Bloomington, IN, and her M.A. and Ph.D. from the University of Oregon, Eugene, OR. Following a unique postdoctoral fellowship in a National Eye Institute program to provide intensive clinical training to scientists, she moved to the University of Pittsburgh Medical Center and Carnegie-Mellon University, where she added research in eye movements, audition, and the vestibular system to her background in vision and tactile research. In 1987, she started a laboratory at the Schepens Eye Research, Harvard University, Boston, Massachusetts, where she developed retinal imaging technologies. She moved her laboratory to Indiana University in 2005, and also founded Aeon Imaging, LLC, to lower costs in healthcare and education. The main focus of Ann's research has been to develop retinal imaging and visual function techniques to combat vision loss. She has introduced novel laser sources into imaging instruments with scanning designs, greatly enlarging the wavelength range available to probe pigments and fluorophores. She demonstrated the properties of normal and diseased tissues by using confocal and multiply scattered light techniques, as well as contrast agents such as sodium fluorescein and indocyanine green, with a goal of improving treatment for retinal disease. She developed specialized techniques for presenting visual stimuli, with invisible near infrared imaging providing a live and surprisingly clear view of the patient's retina while stimuli were displayed. New image processing techniques included analysis for multiply scattered light and polarization, which revealed structures previously unseen in living eyes. In recognition of her work, Ann Elsner is a Fellow of the Optical Society of America and the 2018 Edwin H. Land medalist, a Gold Fellow of the Association for Research in Vision and Ophthalmology, and a Fellow of the American Academy of Optometry.